AD_____
(Leave blank)

Award Number:
(Enter Army Award number assigned to research, i.e., DAMD17-00-1-0296)
W81XWH-09-1-0528

TITLE:
(Enter title of award)
Autophagy Signaling in Prostate Cancer: Identification of a Novel Phosphatase

PRINCIPAL INVESTIGATOR:
(Enter the name and degree of Principal Investigator and any Associates)
Jeffrey P. MacKeigan, Ph.D.

CONTRACTING ORGANIZATION:
(Enter the Name, City, State and Zip Code of the Contracting Organization)
Van Andel Research Institute
Grand Rapids, Michigan 49503

REPORT DATE:
(Enter month and year, i.e., January 2001)
August 2011

TYPE OF REPORT:
(Enter type of report, i.e., annual, midterm, annual summary, final)
Annual

PREPARED FOR: U.S. Army Medical Research and Materiel Command
Fort Detrick, Maryland 21702-5012

REPORT DOCUMENTATION PAGE

Form Approved
OMB No. 0704-0188

1. REPORT DATE *(DD-MM-YYYY)*	**2. REPORT TYPE**	**3. DATES COVERED** *(From - To)*
1 August 2011	ANNUAL	23 JULY 2010 - 22 JULY 2011

4. TITLE AND SUBTITLE

Autophagy Signaling in Prostate Cancer: Identification of a Novel Phosphatase

5a. CONTRACT NUMBER

5b. GRANT NUMBER
W81XWH-09-1-0528

5c. PROGRAM ELEMENT NUMBER

6. AUTHOR(S)

Jeffrey P. MacKeigan, Ph.D.

5d. PROJECT NUMBER

5e. TASK NUMBER

5f. WORK UNIT NUMBER

7. PERFORMING ORGANIZATION NAME(S) AND ADDRESS(ES)

Van Andel Research Institute
Grand Rapids, MI 49503

8. PERFORMING ORGANIZATION REPORT NUMBER

9. SPONSORING / MONITORING AGENCY NAME(S) AND ADDRESS(ES)

U.S. Army Medical Research and Materiel Command
504 Scott Street
Fort Detrick, MD 21702

10. SPONSOR/MONITOR'S ACRONYM(S)

11. SPONSOR/MONITOR'S REPORT NUMBER(S)

12. DISTRIBUTION / AVAILABILITY STATEMENT

Approved for public release; distribution unlimited

13. SUPPLEMENTARY NOTES

14. ABSTRACT

Phosphatidylinositol-3-phosphate (PI(3)P) is concentrated on autophagic vesicles and recruits effector proteins critical for this process. The production of PI(3)P by the class III phosphatidylinositol 3-kinase (PI3K), Vps34, has been well established; however, phosphatases which antagonize this early step in autophagy are not clear. To identify such enzymes, we screened human phosphatase genes by RNA interference (RNAi) and found that loss of PTPsigma, a dual-domain protein tyrosine phosphatase (PTP), increases cellular PI(3)P. Accordingly, we discovered that loss of PTPsigma hyperactivates both constitutive and induced autophagy. Finally, we found that PTPsigma localizes to PI(3)P-positive membranes in cells and this vesicular localization is enhanced during autophagy. Our findings propose a novel role for PTPsigma and provide insight into the regulation of autophagy. Mechanistic knowledge of this process is critical for understanding and targeting therapies for several human diseases, including prostate cancer, in which abnormal autophagy may be pathological.

15. SUBJECT TERMS

Autophagy, Prostate Cancer, Phosphatase, Lipid Signaling

16. SECURITY CLASSIFICATION OF:			**17. LIMITATION OF ABSTRACT**	**18. NUMBER OF PAGES**	**19a. NAME OF RESPONSIBLE PERSON**
a. REPORT	**b. ABSTRACT**	**c. THIS PAGE**			Nicole Doppel
U	U	U	UU	33	**19b. TELEPHONE NUMBER** *(include area code)* 616.234.5654

Table of Contents

INTRODUCTION:

The concept of prostate tumor development as a multi-step process has been well documented. Analysis of human prostate cancer specimens has revealed a variety of deviant tissue states, from early carcinomas and highly malignant tissue, to invasive carcinoma and distant metastases. The many steps of prostate cancer tumor progression are evident from the accumulation of mutant genes in cells as they evolve from a benign state to a malignant state. The loss of PTEN (chromosome 10q), pRB (chromosome 13q) and p53 (chromosome 17p) is coupled with a large percentage of tumors harboring Myc amplifications, AR mutations and Bcl-2 overexpression [1-3]. In agreement with this, our data indicate a stage or metastasis-dependent loss of PTPsigma (PTPRS) mRNA. These data suggest that PTPsigma may be involved in prostate progression, perhaps through activation of autophagy after loss of PTPsigma.

BODY:

Aim #1: Identify the catalytic mechanism whereby PTPRS regulates PI(3)P levels.

We have completed the following tasks associated with the Statement of Work. Figures referenced for all tasks include unpublished data (Figures 1-3 in the *Supplementary Data*) as well as those published within the article attached in *Supplementary Data* [4]. We have generated PTPRS constructs containing catalytically inactive point mutations in the D1 (C1589S and C1589A), D2 (C1880S), and both D1 and D2 PTP domains (task 1) (**Fig. 1A**). These mutations have been sequence-verified and characterized for phosphatase activity *in vitro* (task 2). The constructs have been inserted in bacterial vectors (pGEXKG) for recombinant protein purification as well as mammalian expression vectors (PTPRS in full-length and a truncated form containing the transmembrane and cytosolic residues). We measured PTPRS activity using a phospho-tyrosine (pTyr) peptide with malachite green free phosphate detection to verify catalytic activity residues exclusively within the D1 domain (**Fig. 1B**). We cannot detect robust PI(3)P-phosphatase activity using standard assays (**Fig. S3 [4]**).

We have also completed the autophagy assays that include LC3 Western blots (task 4) and immunofluorescence for endogenous LC3 (task 5) (**Figs. 1, 2, S2 [4]**). We have monitored autophagic vesicles by electron microscopy (task 6) at the Michigan State University Center for Advanced Microscopy (**Fig. 3 [4]**). We have also quantified the number of autophagic vesicles per cell for both cells containing wild-type PTPRS and those subjected to siRNA-mediated knockdown of PTPRS (task 7) (**Figs. 2, S2 [4]**). This work is described in more detail within the attached referenced article. For this Aim, the remaining task (task 3) includes testing the mutants in C4-2B cells to determine the necessity of the active site in prostate cancer cells, as compared to immortalized normal PEC36 prostate cells. We have measured autophagy in a panel of metastatic prostate cancer cell lines as preliminary effort to this goal (**Fig. 2**).

Aim #2: Determine the regulation and subcellular localization of PTPRS during autophagy.

We have completed the following tasks associated with the Statement of Work. We have cloned and expressed full-length, untagged PTPRS which we detect by standard immunoblotting protocols using a D1-targeted (C-terminal) monoclonal antibody (task 1). This is a refinement of the original approach which involved a C-terminal V5 epitope tag. We have analyzed PTPRS processing in U2OS cells where we found that a C-terminal fragment (CTF) is constitutively turned over in the lysosome in the presence of full-nutrients (**Fig. 3A)**. The formation of this CTF is blocked by Batimastat, an extracellular metalloprotease inhibitor, suggesting it is

generated following cleavage (**Fig. 3B**). Upon autophagy induction (by amino acid starvation), a further processed fragment is formed which we predict is an intracellular domain (ICD) (**Fig. 3C**).

We have performed numerous autophagy assays (task 2, task 3, task 4) (**Fig. 2; Figs. 1-3, S2 [4]).** We have monitored PTPRS localization using standard immunofluorescence microscopy. We have introduced full-length, untagged PTPRS into U2OS cells and followed the C-terminus using D1-targeted monoclonal antibodies (task 5). Again, this is a refinement of the original approach using C-terminal V5-tagged PTPRS. We have compared PTPRS distribution to both EGFP-2xFYVE and RFP-labeled LC3 to find PTPRS on both PI(3)P and LC3-positive vesicles (task 6) (**Figs. 4, 5, S3 [4]**). We have assessed the enrichment of PTPRS in an autophagic fraction during autophagy by comparing cells cultured in full nutrients to those starved of amino acids (task 8). For this Aim, several tasks remain to be completed. One task includes the isolation of autophagosomes by differential centrifugation from cells (task 7). A published protocol has been identified and pilot studies are underway. Further, immunogold electron microscopy can be utilized to further define the subcellular localization of PTPRS (task 9, task 10). We have established a relationship with the transmission electron microscopy core at Michigan State University Center for Advanced Microscopy and are familiar with protocols to accomplish these tasks.

Specific Aim #3: Establish the role of PTPRS in prostate cancer chemoresistance.
In this Aim, we will evaluate the role of PTPRS in prostate cancer chemoresistance using an androgen-independent C4-2B metastatic model of prostate cancer. We will generate stable C4-2B cell lines expressing EGFP (task 1). CB17 SCID will be injected with EGFP-positive C4-2B cells into the prostate gland (task 2). Tumors will be allowed to grow for 10 weeks, at which time the mice will be randomly assigned to one of four groups of ten mice. Each group of mice will then be treated by intraperitoneal injection with control, docetaxel (low dose, 10 mg/kg) or docetaxel (high dose, 60 mg/kg), respectively (task 3). Animal health will be monitored daily (task 4). Injections will continue every week for three weeks (injections on days 1, 7, 14, and 21 for a total of 4 injections) at which time the mice will be euthanized and the tumors will be dissected (task 5). Half of each tumor will be paraffin embedded, and half of the tumor will be frozen for later analysis (task 6). Lungs will be excised, fixed, and lung metastasis quantified (task 7). We will measure 25 sections (20 μm thick) from the apex to the base of the lung for the presence of metastasis. The general strategy of the PTPRS C to S mutant experimental approach is to inject stable clones expressing high levels of PTPRS or PTPRS C1589S or C1880S (task 8). Injected cells will then be allowed to establish tumors for 10 weeks. Established tumors will then be treated by intraperitoneal injection of docetaxel (task 9). Tumors will also be treated with vehicle control as a negative control. Immunohistochemistry and western blot (anti-V5 antibody) for V5-PTPRS will be used to confirm expression levels (task 10). To drive refinement of the model, pilot studies have been designed. Protocols for these tasks have been submitted to the IACUC committee at VAI and have been approved. Kinetics of both autophagy-modulating compounds (rapamycin, chloroquine, bafilomycin A1) and chemotherapeutics (taxol, cisplatin, etoposide) have been investigated in a number of metastatic prostate cancer lines *in vitro* (including LNCaP, C4-2B, DU145, and PC3) (**Table 1**).

After successful completion of the orthotopic lung metastatic model, we will use the C4-2B-EGFP cells and intratibial inoculation to quantify tumor burden in a metastatic relevant site after systemic chemotherapy (task 11). Tumor burden will be quantified on days 10, 17, and 24 after injection of the tumor cells (task 12). Whole body fluorescent images will be obtained using our whole animal bioluminescence equipment in the injected tibiae. Again, mice injected intratibial with either wild-type PTPRS or the C to S mutant; and mice will be treated with docetaxel as described above (task 13). The immunohistochemistry staining will be performed (task 14). One section from each prostate tumor and lung metastases will be stained, scanned, and digital images obtained for proliferation (PCNA, Ki67) and apoptosis (activated caspase 9). Protocols have been written, submitted, and approved for this work. Optimization of this technique and pilot studies are underway.

KEY RESEARCH ACCOMPLISHMENTS:

- RNAi screen identifies PTPsigma as a modulator of PI(3)P signaling
- Loss of PTPsigma hyperactivates constitutive and induced autophagy
- PTPsigma localizes to PI(3)P-positive vesicles and rescues the siRNA phenotype
- The vesicular localization of PTPsigma does not require PI(3)P
- PTPsigma harbors robust protein tyrosine phosphatase activity, but not PI(3)P-phosphatase activity, and this is harbored within the D1 PTP domain
- PTPsigma is processed into a CTF during constitutive autophagy and targeted to the lysosome
- PTPsigma is processed into a putative ICD during starvation-induced autophagy

REPORTABLE OUTCOMES:

Martin KR, Xu Y, Looyenga BD, Davis RJ, Wu CL, Tremblay ML, Xu HE, MacKeigan JP (2011). Identification of PTPsigma as an autophagic phosphatase. *J Cell Sci*. 2011 Mar 1;124(Pt 5):812-9.

He Y, Xu Y, Zhang C, Gao X, Dykema KJ, Martin KR, Ke J, Hudson EA, Khoo SK, Resau JH, Alberts AS, MacKeigan JP, Furge KA, Xu HE. Identification of a lysosomal pathway that modulates glucocorticoid signaling and the inflammatory response. *Sci Signal.* 2011 Jul 5;4(180):ra44

CONCLUSION:

Through use of a high-content cell-based RNAi screen, we have identified phosphatases whose knockdown elevates cellular PI(3)P. Notably, RNAi-mediated knockdown of MTMR6 and several other phosphatases resulted in swollen and often perinuclear PI(3)P-positive vesicles. Previous studies have shown similar phenotypes when endocytic PI(3)P is elevated, for example, by constitutive activation of early endosomal Rab5, or knockdown of the PI5-kinase, PIKfyve [5, 6]. Accordingly, the vesicles observed following knockdown of these phosphatases are likely endosomal and these enzymes, including MTMR6, may function in endocytic signaling. Of note, knockdown of both PTPN11 (SHP2) and PTPN13 (PTPL1) resulted in increased EGFP-2xFYVE punctae (Table 2.1). PTPN13, a phosphatase proposed to have both tumor suppressive and

oncogenic functions, has been implicated in several signal transduction pathways. Specifically, PTPN13 was shown to inhibit PI3K/Akt signaling and thus, the PI(3)P phenotype elicited by knockdown could potentially be explained by altered 3'-phosphoinositide metabolism [7, 8]. Mutations in SHP2 are associated with several human diseases, most notably Noonan syndrome, LEOPARD syndrome, and juvenile myelomonocytic leukemia [9-12]. Its activity has been linked to numerous signaling pathways, often downstream of receptor tyrosine kinases, and the observed phenotype could be a consequence of disruption of any number of substrates [13].

Surprisingly, we did not identify MTMR3 or MTMR14 (hJumpy), the PI(3)P-phosphatases with reported roles in autophagy. The myotubularin phosphatases comprise a large, highly conserved family of enzymes whose members have been shown to function as heteromeric partners [14]. As one example, MTMR3 and MTMR4, both FYVE-domain containing phosphatases, have been demonstrated to interact and inhibit PI(3)P [14]. Accordingly, gene-by-gene loss of function analysis of this family may not reveal phenotypes if compensation within the family occurs. Further, these enzymes may serve cell- or context-specific functions not revealed in this study.

The most striking result from this study was the presence of abundant PI(3)P-positive vesicles following PTPsigma knockdown which phenocopied that of an autophagic cell. We confirmed hyperactive autophagy in the absence of PTPsigma through use of multiple autophagy markers, as well as electron microscopy. Atg12 and LC3-positive autophagic vesicles were substantially more abundant in the absence of PTPsigma when cells were cultured in full nutrients (constitutive AVs) or treated with rapamycin (induced AVs). These autophagic vesicles accumulated upon treatment with the lysosomal inhibitors, Baf-A1 and chloroquine, demonstrating that they were functional and destined for lysosomal degradation. This phenotype suggests PTPsigma regulates an early step in autophagy induction and its loss results in increased autophagic vesicle generation. This is consistent with the fact that PI(3)P is generated on early phagophores and is required for proper autophagic vesicle formation. A role for PTPsigma in autophagy induction and specifically, PI(3)P regulation, is supported by our findings that PTPsigma localizes to PI(3)P-positive vesicles which increase in number during autophagy.

It remains to be addressed how PTPsigma is targeted to autophagic vesicles. PTPsigma is expressed at the cell surface in a two subunit complex comprised of a large ectodomain and a membrane-spanning intracellular domain. Accordingly, it is implicated in cell-cell and cell-ECM interactions, and it is a critical regulator of axon homeostasis and neuronal development [15-18]. Relevant to our own work, ectodomain shedding and internalization of a membrane-bound carboxy-terminal fragment has been demonstrated previously [18]. Through immunofluorescent analysis of PTPsigma using D1 domain-specific antibodies, we place intracellular PTPsigma on PI(3)P-positive autophagic vesicles. Autophagosomes frequently fuse with endosomes during their maturation, forming hybrid organelles called amphisomes, establishing the possibility that PTPsigma is internalized by endocytosis to arrive at autophagic vesicles [19]. Further, the close relative of PTPsigma, LAR (PTPRF), undergoes an additional proteolytic event whereby a soluble intracellular domain is formed and targeted inside the cell, similar to the Notch receptor [20]. PTPsigma contains similar cleavage residues to LAR, making it therefore plausible that PTPsigma is targeted from the plasma membrane to autophagic vesicles through a series of proteolytic events in response to autophagic stimuli. Thus, this phosphatase may serve several

unique functions during various cellular conditions which are governed by its subcellular localization.

A critical finding presented here is the recruitment of PTPsigma to vesicular structures during amino acid-starvation which occurs even in the absence of PI(3)P generation. This finding, together with the hyperactivation of autophagy elicited by PTPsigma knockdown (as measured by PI(3)P, Atg12, and LC3), suggests PTPsigma regulates autophagy at an early step upstream of this lipid. In further support of this, we found that while almost all PTPsigma-positive vesicles are also positive for PI(3)P (EGFP-2xFYVE presence), fewer harbored LC3, a marker which is incorporated into AVs at later maturation stages.

There are several potential mechanisms by which PTPsigma may function to regulate autophagy. First, it is possible that PTPsigma could directly dephosphorylate PI(3)P following recruitment to AVs. We did test the activity of recombinant PTPsigma in vitro, and while we could not detect PI(3)P-phosphatase activity, it cannot be entirely excluded that PI(3)P does not serve as a direct substrate *in vivo* (Figure 2.9). It is also possible that PTPsigma uses its robust protein phosphatase activity to regulate the function of a PI(3)P-modifying enzyme, such as a PI(3)P-phosphatase or a PI(4)- or PI(5)-kinase. Alternatively, PTPsigma could control the activity of Vps34, which contains at least one phosphotyrosine site, or another component within the larger Vps34 complex [21]. Finally, PTPsigma may contribute to the regulation of autophagy at the earliest initiation step, which is executed by a complex of autophagy proteins, namely ULK1 (Atg1) and Atg13. The functional formation of this complex, which permits the generation of the PI(3)P-positive phagophore, was recently found to be tightly regulated by phosphorylation events [22-25]. The aim of future work will be to determine the precise mechanism by which PTPsigma functions to regulate autophagy.

Finally, we found that PTPsigma was processed from its P-subunit into a putative C-terminal fragment (CTF). This processing occurs under normal growth conditions and results in CTF targeting and turnover in the lysosome. Further, we uncovered evidence that PTPsigma is processed into a fragment smaller than the CTF during starvation-induced autophagy. This fragment does not appear to be targeted to the lysosome and while it is logical to assume it is an ICD, its molecular weight is smaller than that reported for a LAR ICD [26]. PTPsigma does in fact have residues within and just C-terminal to its transmembrane domain that are similar to those in Notch required for gamma-secretase-mediated ICD formation [27]. However, mutation of the analogous residues in LAR did not impair the ability of gamma secretase to generate an ICD so they may not be critical for a PTPsigma-ICD either [26]. If this detected fragment is in fact an ICD, it may be generated through a unique mechanism or from a site downstream of its transmembrane domain, resulting in a smaller size. Regardless, because PTPsigma exerts its inhibitory effect on autophagy in the presence of nutrients, it is likely that the CTF is the fragment relevant to PI(3)P suppression. The fact that the CTF is membrane-bound and turned over in the lysosome supports a model where PTPsigma is processed and internalized from the cell surface as part of the endocytic pathway. It would likely be during this trafficking that PTPsigma resides on PI(3)P-positive endocytic vesicles and likely suppresses VPS34 signaling to impede the maturation of both endosomal and autophagic vesicles.

REFERENCES:

1. Ittmann, M.M., *Chromosome 10 alterations in prostate adenocarcinoma (review).* Oncol Rep, 1998. **5**(6): p. 1329-35.

2. Li, J., et al., *PTEN, a putative protein tyrosine phosphatase gene mutated in human brain, breast, and prostate cancer.* Science, 1997. **275**(5308): p. 1943-7.

3. Feldman, B.J. and D. Feldman, *The development of androgen-independent prostate cancer.* Nat Rev Cancer, 2001. **1**(1): p. 34-45.

4. Martin, K.R., et al., *Identification of PTPsigma as an autophagic phosphatase.* J Cell Sci, 2011. **124**(Pt 5): p. 812-9.

5. Murray, J.T., et al., *Role of Rab5 in the recruitment of hVps34/p150 to the early dosome.* Traffic, 2002. **3**(6): p. 416-27.

6. Rutherford, A.C., et al., *The mammalian phosphatidylinositol 3-phosphate 5-kinase (PIKfyve) regulates endosome-to-TGN retrograde transport.* J Cell Sci, 2006. **119**(Pt 19): p. 3944-57.

7. Abaan, O.D. and J.A. Toretsky, *PTPL1: a large phosphatase with a split personality.* Cancer Metastasis Rev, 2008. **27**(2): p. 205-14.

8. Dromard, M., et al., *The putative tumor suppressor gene PTPN13/PTPL1 induces apoptosis through insulin receptor substrate-1 dephosphorylation.* Cancer Res, 2007. **67**(14): p. 6806-13.

9. Mohi, M.G. and B.G. Neel, *The role of Shp2 (PTPN11) in cancer.* Curr Opin Genet Dev, 2007. **17**(1): p. 23-30.

10. Kontaridis, M.I., et al., *PTPN11 (Shp2) mutations in LEOPARD syndrome have dominant negative, not activating, effects.* J Biol Chem, 2006. **281**(10): p. 6785-92.

11. Mohi, M.G., et al., *Prognostic, therapeutic, and mechanistic implications of a mouse model of leukemia evoked by Shp2 (PTPN11) mutations.* Cancer Cell, 2005. **7**(2): p. 179-91.

12. Araki, T., et al., *Mouse model of Noonan syndrome reveals cell type- and gene dosage-dependent effects of Ptpn11 mutation.* Nat Med, 2004. **10**(8): p. 849-57.

13. Chan, G., D. Kalaitzidis, and B.G. Neel, *The tyrosine phosphatase Shp2 (PTPN11) in cancer.* Cancer Metastasis Rev, 2008. **27**(2): p. 179-92.

14. Lorenzo, O., S. Urbe, and M.J. Clague, *Systematic analysis of myotubularins: heteromeric interactions, subcellular localisation and endosome related functions.* J Cell Sci, 2006. **119**(Pt 14): p. 2953-9.

15. Elchebly, M., et al., *Neuroendocrine dysplasia in mice lacking protein tyrosine phosphatase sigma.* Nat Genet, 1999. **21**(3): p. 330-3.

16. Wallace, M.J., et al., *Neuronal defects and posterior pituitary hypoplasia in mice lacking the receptor tyrosine phosphatase PTPsigma.* Nat Genet, 1999. **21**(3): p. 334-8.

17. Uetani, N., et al., *Mammalian motoneuron axon targeting requires receptor protein tyrosine phosphatases sigma and delta.* J Neurosci, 2006. **26**(22): p. 5872-80.

18. Aicher, B., et al., *Cellular redistribution of protein tyrosine phosphatases LAR and PTPsigma by inducible proteolytic processing.* J Cell Biol, 1997. **138**(3): p. 681-96.

19. Klionsky, D.J., *Autophagy: from phenomenology to molecular understanding in less than a decade.* Nat Rev Mol Cell Biol, 2007. **8**(11): p. 931-7.

20. Ruhe, J.E., et al., *EGFR signaling leads to downregulation of PTP-LAR via TACE-mediated proteolytic processing.* Cell Signal, 2006. **18**(9): p. 1515-27.

21. Imami, K., et al., *Automated phosphoproteome analysis for cultured cancer cells by two-dimensional nanoLC-MS using a calcined titania/C18 biphasic column.* Anal Sci, 2008. **24**(1): p. 161-6.

22. Chang, Y.Y. and T.P. Neufeld, *An Atg1/Atg13 complex with multiple roles in TOR-mediated autophagy regulation.* Mol Biol Cell, 2009. **20**(7): p. 2004-14.

23. Ganley, I.G., et al., *ULK1.ATG13.FIP200 complex mediates mTOR signaling and is essential for autophagy.* J Biol Chem, 2009. **284**(18): p. 12297-305.

24. Hosokawa, N., et al., *Nutrient-dependent mTORC1 association with the ULK1-Atg13-FIP200 complex required for autophagy.* Mol Biol Cell, 2009. **20**(7): p. 1981-91.

25. Jung, C.H., et al., *ULK-Atg13-FIP200 complexes mediate mTOR signaling to the autophagy machinery.* Mol Biol Cell, 2009. **20**(7): p. 1992-2003.

26. Haapasalo, A., et al., *Presenilin/gamma-secretase-mediated cleavage regulates association of leukocyte-common antigen-related (LAR) receptor tyrosine phosphatase with beta-catenin.* J Biol Chem, 2007. **282**(12): p. 9063-72.

27. Gupta-Rossi, N., et al., *Monoubiquitination and endocytosis direct gamma-secretase cleavage of activated Notch receptor.* J Cell Biol, 2004. **166**(1): p. 73-83.

APPENDICES:

DD FORM 882

SUPPORTING DATA:

Figure 1

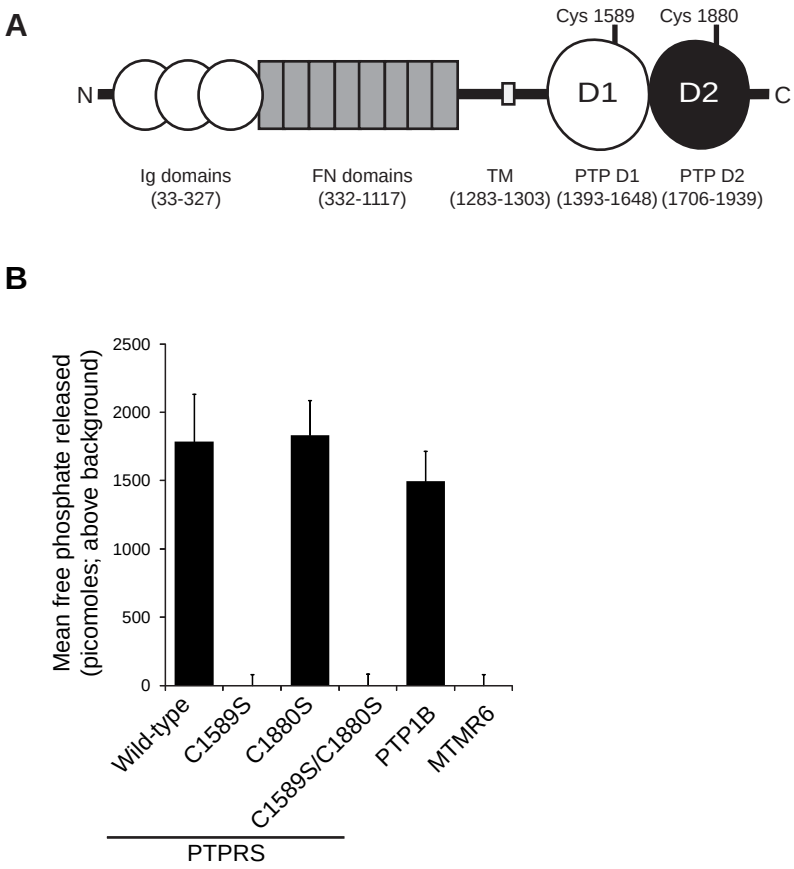

Figure 1. PTPRS mutant design and characterization. (A) PTPsigma consists of an N-terminal ectodomain made of (3) immunoglobulin (Ig)-like repeats and fibronectin (FN) type III-like repeats (up to 8 in the longest isoform). A single transmembrane domain precedes two C-terminal cytosol-facing phosphatase domains, termed D1 and D2. To generate catalytically inactive mutants, we mutate the D1 active site cysteine (C1589) and/or D2 active site cysteine (C1880) to serines. (**B**) PTPRS in wild-type, D1 inactive (C1589S), D2 inactive (C1880S), or D1 and D2 inactive (C1589S/C1880S) was purified recombinantly using pGEXKG expression vectors and bacteria. Enzymes were tested for phosphatase activity *in vitro* using a 100 uM phosphotyrosine peptide substrate and malachite green detection of released free phosphates. Activity is expressed as picomoles free phosphate released from the substrate during a 15 minute reaction (enzyme-only and substrate-only values subtracted). Bars represent standard deviation. Recombinant PTP1B and MTMR6 (a PI(3)P-phosphatase) were used as positive and negative PTP controls, respectively.

Figure 2

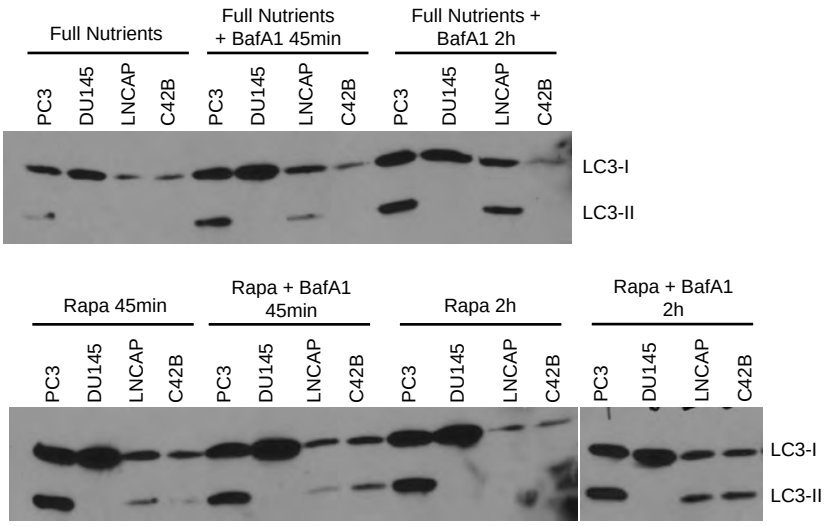

Figure 2. Autophagic flux in metastatic prostate cancer cell lines. Autophagic flux was measured by standard immunoblotting for LC3 processing using whole cell lysates from a panel of metastatic prostate cancer cell lines (LNCaP, C4-2B, DU145, PC3). Prior to cell lysis, cells were treated with full nutrients with or without 100 nM bafilomycin A1 (BafA1; to inhibit lysosomes and LC3 turnover) for 45 min or 2 h, as indicated. Alternatively, cells were treated with 50 nM rapamycin (Rapa) for 45 min or 2 h with or without BafA1, as indicated. Endogenous LC3-I (cytosolic) and LC3-II (autophagic) was detected using antibodies.

Figure 3

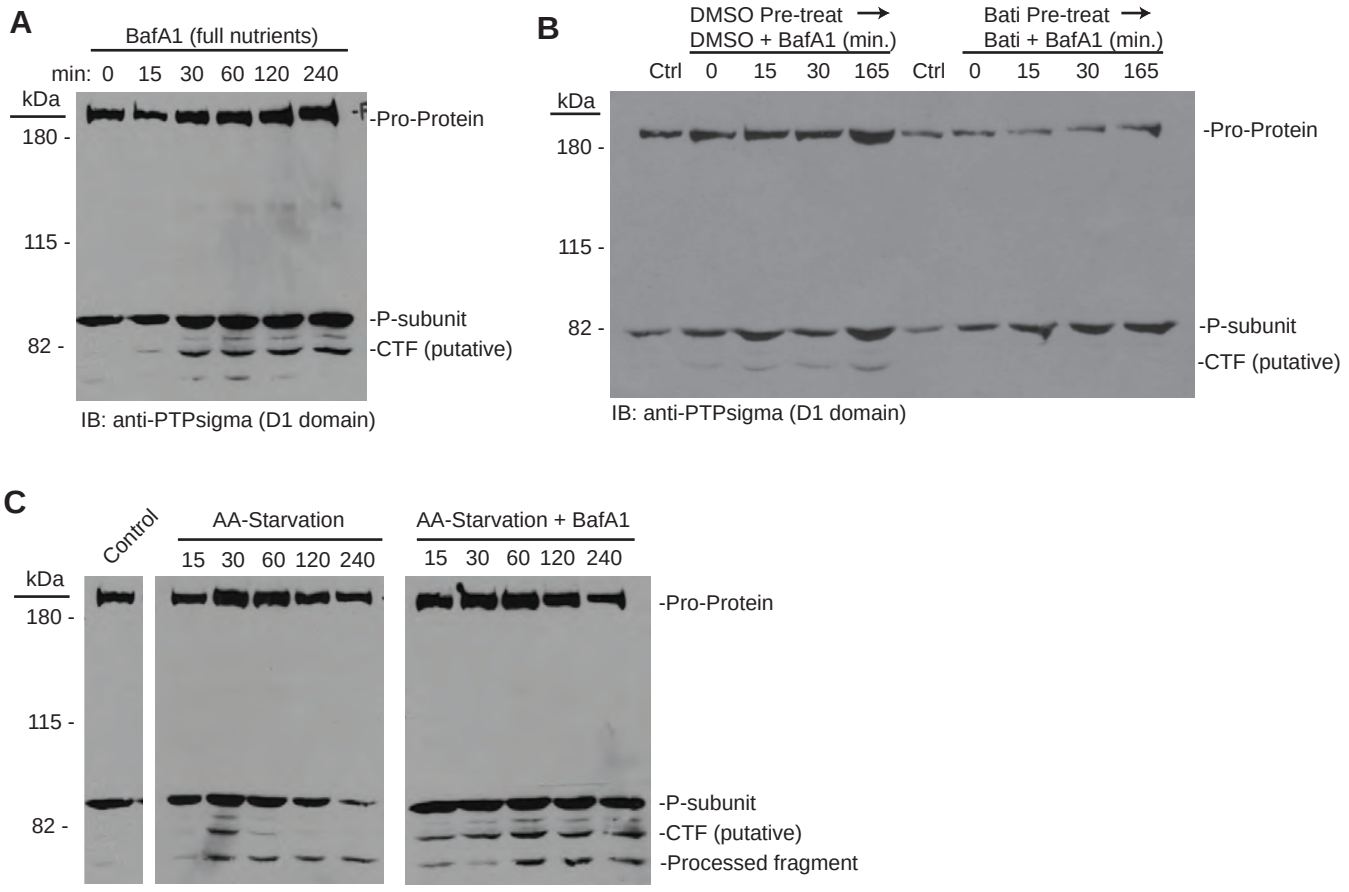

Figure 3. Proteolytic processing of PTPsigma. (A-B) A PTPsigma C-terminal fragment (CTF) is generated and processed in a lysosomal pathway. (A) U2OS cells expressing full-length untagged PTPsigma (FL-PTPsigma) were treated with bafilomycin A1 (BafA1), a lysosomal inhibitor, for 0 to 240 minutes. Lysates were probed by western blot with D1-targeted PTPsigma antibodies. (B) U2OS cells expressing FL-PTPsigma were pre-treated with Batimastat (Bati), an extracellular metalloprotease inhibitor, or DMSO (vehicle) for 4 hrs then supplemented with BafA1 for the indicated times. Lysates were probed by western blot with D1-targeted PTPsigma antibodies. **(C)** U2OS cells expressing FL-PTPsigma were amino acid-starved to induce autophagy for the times indicated in the absence (left) or presence (right) of BafA1. Lysates were probed by western blot with D1-targeted PTPsigma antibodies.

Table 1

The above results were generated following exposure to a panel of chemical compounds (Rapamycin, Chloroquine, Bafilomycin A1, Taxol, Cisplatin, and Etoposide). The doses administered for Rapamycin, Bafilomycin, and Taxol were in the 0-500 nM range while a 0-500 µM range was utilized for Chloroquine, Cisplatin, and Etoposide. In total, nine doses of each drug were tested in these metastatic prostate cancer lines (C42B, LNCaP, PC3, DU145). 48h post treatment, Cell Titer Glo was used as a readout of cell viability. All data was normalized to an untreated control of the appropriate line. SigmaPlot software was used to establish EC_{50} doses.

	C4-2B	**LNCaP**	**PC3***	**DU145***
Rapamycin	>0.5 µM	>0.5 µM	>0.5 µM	>0.5 µM
Chloroquine	20 µM	50 µM	60 µM	96.3 µM
Bafilomycin A1	>0.5 µM	60 nM	375 nM	>0.5 µM
Taxol	10 nM	>500 nM	475 nM	55.9 nM
Cisplatin	10 µM	30 µM	7.5 µM	510 nM
Etoposide	60 µM	300 µM	150 µM	3.1 µM

* - in triplicate

Identification of PTPs as an autophagic phosphatase

Katie R. Martin[1,2], Yong Xu[3], Brendan D. Looyenga[1], Ryan J. Davis[1], Chia-Lun Wu[4], Michel L. Tremblay[4], H. Eric Xu[3] and Jeffrey P. MacKeigan[1,*]

[1]Laboratory of Systems Biology, Van Andel Research Institute, Grand Rapids, MI 49503, USA
[2]Cell and Molecular Biology Graduate Program, Michigan State University, East Lansing, MI 48824-4320, USA
[3]Laboratory of Structural Sciences, Van Andel Research Institute, Grand Rapids, MI 49503, USA
[4]Goodman Cancer Centre, Department of Biochemistry, McGill University, Montreal, QC H3A 1A3, Canada
*Author for correspondence (jeff.mackeigan@vai.org)

Accepted 9 November 2010
Journal of Cell Science 124, 812-819

doi:10.1242/jcs.080341

Summary

Macroautophagy is a dynamic process whereby portions of the cytosol are encapsulated in double-membrane vesicles and delivered to the lysosome for degradation. Phosphatidylinositol-3-phosphate (PtdIns3*P*) is concentrated on autophagic vesicles and recruits effector proteins that are crucial for this process. The production of PtdIns3*P* by the class III phosphatidylinositol 3-kinase Vps34, has been well established; however, protein phosphatases that antagonize this early step in autophagy remain to be identified. To identify such enzymes, we screened human phosphatase genes by RNA interference and found that loss of PTPs, a dual-domain protein tyrosine phosphatase (PTP), increases levels of cellular PtdIns3*P*. The abundant PtdIns3*P*-positive vesicles conferred by loss of PTPs strikingly phenocopied those observed in cells starved of amino acids. Accordingly, we discovered that loss of PTPs hyperactivates both constitutive and induced autophagy. Finally, we found that PTPs localizes to PtdIns3*P*-positive membranes in cells, and this vesicular localization is enhanced during autophagy. We therefore describe a novel role for PTPs and provide insight into the regulation of autophagy. Mechanistic knowledge of this process is crucial for understanding and targeting therapies for several human diseases, including cancer and Alzheimer's disease, in which abnormal autophagy might be pathological.

Key words: FYVE, PTPs, PtdIns3*P*, RNAi, Autophagy, Phosphatase

Introduction

In addition to the well-characterized role of phosphatidylinositol-3-phosphate (PtdIns3*P*) in endocytosis, recent evidence has uncovered a crucial requirement for this lipid in macroautophagy (autophagy) (Axe et al., 2008; Obara et al., 2008a; Petiot et al., 2000). Autophagy occurs constitutively in nearly all cells to maintain homeostasis, but is further activated in response to stress as a survival or adaptive mechanism. During autophagy, a double-membrane phagophore forms and elongates around portions of cytosol, matures into an enclosed autophagosome, and delivers its contents to the lysosome for degradation (Klionsky, 2007). Basic biochemical components (i.e. amino acids and fatty acids) are exported from the lysosome and recycled by the cell, representing an energetically favorable alternative to de novo synthesis. In mammalian systems, the lipid kinase Vps34 forms a complex with several proteins, including Vps15, Beclin1, Atg14L, UVRAG and Bif1 to generate PtdIns3*P* on autophagic vesicles (Itakura et al., 2008; Zhong et al., 2009). PtdIns3*P* then recruits and tethers effector proteins, such as WIPI-1 (Atg18), which are required for proper membrane formation (Obara et al., 2008b; Proikas-Cezanne et al., 2004). The crucial requirement for PtdIns3*P* in this process is evidenced by the fact that autophagy is ablated in mutant Vps34 yeast strains and genetic Vps34 knockouts in *Drosophila* (Juhasz et al., 2008; Kihara et al., 2001). Despite knowledge of PtdIns3*P* production, the antagonistic phosphatases that regulate PtdIns3*P* during autophagy have remained elusive. Two myotubularin-related phosphatases, MTMR3 and MTMR14 (hJumpy), have recently been shown to dephosphorylate autophagic PtdIns3*P* in various contexts (Taguchi-Atarashi et al., 2010; Vergne et al., 2009). However, given the complexity of autophagy execution and the number of proteins in the autophagy network, we predict that additional protein phosphatases exist to regulate this process. Accordingly, we performed a high-content cell-based RNAi screen using a fluorescent PtdIns3*P* sensor to identify protein phosphatases that function upstream of PtdIns3*P* during autophagy.

Results

RNAi screening identifies PTPs as a modulator of PtdIns3*P* signaling

FYVE (Fab1, YOTB, Vac1 and EEA1) domains are cysteine-rich zinc-finger binding motifs that specifically recognize and bind PtdIns3*P* (Gaullier et al., 1998). An EGFP molecule fused to two tandem FYVE domains, termed EGFP–2xFYVE, serves as an effective cellular sensor of PtdIns3*P* (Gillooly et al., 2000). We analyzed U2OS cells stably expressing this construct by fluorescent microscopy and found that PtdIns3*P* predominantly localized to punctate, often perinuclear, vesicles when cultured in complete growth medium with full nutrients (Fig. 1A, supplementary material Movie 1). RNAi-mediated knockdown of Vps34 reduced cellular PtdIns3*P* content and resulted in a diffuse cytosolic distribution of EGFP–2xFYVE (Fig. 1B,F, supplementary material Fig. S1A). By contrast, a redistribution of EGFP–2xFYVE to small abundant autophagic vesicles occurred when cells were deprived of amino acids to potently induce autophagy (Fig. 1C, supplementary material Movie 2).

To identify genes that downregulate PtdIns3*P* signaling, we used several siRNAs targeting over 200 known and putative human phosphatases. The siRNAs were introduced into U2OS EGFP–2xFYVE cells, and the cells were subsequently monitored

Journal of Cell Science

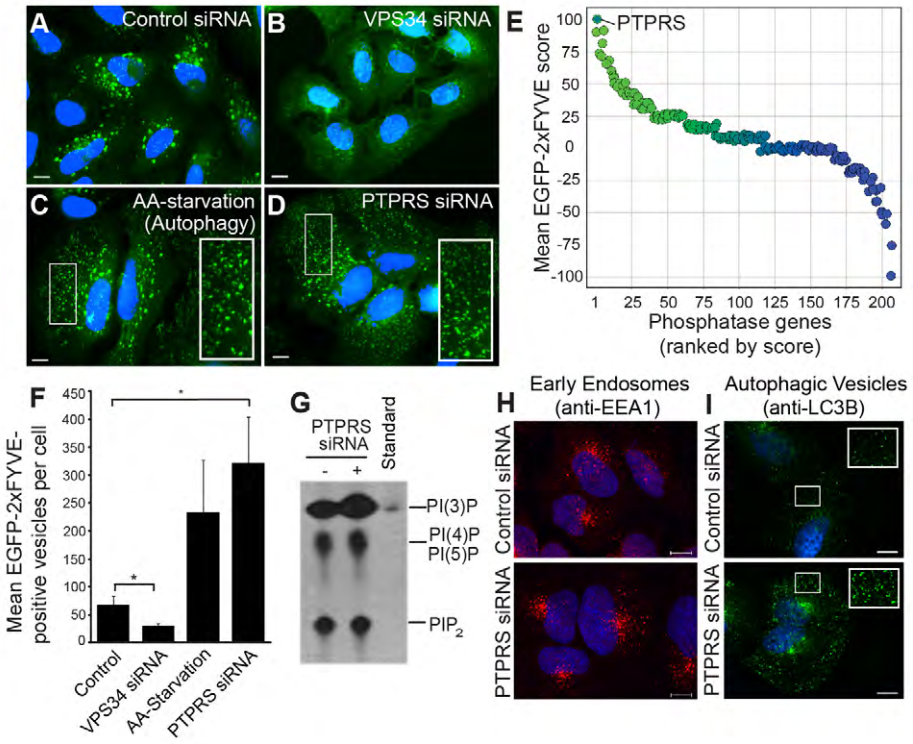

Fig. 1. A cell-based siRNA screen identifies PTPs as a modulator of PtdIns3*P*. (**A–D**) U2OS EGFP–2xFYVE cells transfected with control siRNA (A), *VSP34* siRNA (B), starved of amino acids for 3 hours (C), or transfected with *PTPRS* siRNA (D), were fixed and imaged at 60× magnification by fluorescent microscopy (green, PtdIns3*P*, EGFP–2xFYVE; blue, nuclei). Insets show 2× magnifications of small EGFP–2xFYVE vesicles. Scale bars: 10 µm. (**E**) Following knockdown of phosphatases, EGFP–2xFYVE-positive punctae were scored from –100 (decreased from control cells) to +100 (increased). Phosphatases are ranked and plotted by decreasing score (left to right) with genes whose loss increased EGFP–2xFYVE fluorescence highlighted in green and whose loss caused decreases highlighted in blue. *PTPRS* is identified. (**F**) Mean EGFP–2xFYVE-positive punctate were quantified from cells under the conditions indicated using image analysis software. Bars represent s.e.m.; **P*<0.05. (**G**) Phospholipids were radiolabeled in vivo, extracted, resolved by TLC, and visualized by autoradiography following transfection with control or *PTPRS* siRNA. A radiolabeled PtdIns3*P* standard was resolved adjacent to extracted lipids. (**H**,**I**) Endosomes were labeled by immunostaining with anti-EEA1 antibodies (H) and autophagic vesicles were labeled with anti-LC3B antibodies (I) following transfection with control or *PTPRS* siRNA (red, EEA1; green, LC3B; blue, nuclei). Insets show 2× magnifications of LC3-positive vesicles. Scale bars: 10 µm.

for PtdIns3*P* signaling. We identified several genes whose knockdown significantly increased the abundance of cellular EGFP–2xFYVE punctae (Fig. 1E, supplementary material Table S1). Most notably, PtdIns3*P* was substantially increased following knockdown of the myotubularin family member MTMR6 (supplementary material Fig. S1B,C), as well as the dual-domain protein tyrosine phosphatase PTPRS (PTPs) (Fig. 1D,E). Although reduced expression of MTMR6 was characterized by the appearance of enlarged perinuclear vesicles, the siRNAs targeting PTPs caused a dramatic accumulation of abundant smaller vesicles throughout the cytosol, which phenocopied results observed during amino acid starvation (Fig. 1C,D, supplementary material Movie 3). Quantification of PtdIns3*P*-positive vesicles revealed a 3.5-fold increase in abundance during starvation-induced autophagy and a nearly 5-fold increase caused by knockdown of PTPs alone (Fig. 1F). This phenotype was confirmed using four unique siRNA sequences targeting PTPs (supplementary material Fig. S1D-K).

To validate a physiological increase in PtdIns3*P* following knockdown of PTPs, phospholipids were radiolabeled with [^{32}P]orthophosphate in vivo, extracted, and resolved by thin-layer chromatography. Indeed, PtdIns3*P* levels were specifically elevated in the absence of PTPs, whereas other lipid species remained unchanged (Fig. 1G). To determine the identity of the PtdIns3*P*-positive vesicles formed by knockdown of PTPs, we immunostained cells with well-established markers of early endosomes [anti-EEA1 (early endosomal antigen 1)] and autophagic vesicles (AVs) [anti-LC3 (light chain 3)]. We found that knockdown of PTPs had no substantial effect on the presence of EEA1-positive endosomes (Fig. 1H, supplementary material Fig. S2A), but significantly increased the abundance of LC3-positive vesicles (Fig. 1I). From this, we hypothesized that PTPs functions during autophagy and focused our attention on this enzyme as a candidate autophagic phosphatase.

Loss of PTPs hyperactivates constitutive and induced autophagy

The striking resemblance of PtdIns3*P*-positive vesicles induced by PTPs knockdown to AVs formed during amino acid starvation led us to propose that autophagy is hyperactivated in the absence of PTPs, despite the presence of nutrients. To test this, autophagy was analyzed in U2OS cells by evaluating two ubiquitin-like proteins, Atg12 and LC3 (Atg8), which become conjugated to AVs during autophagy. Following phagophore nucleation, Atg12 covalently binds Atg5 and oligomerizes with Atg16L at the autophagic membrane (Klionsky, 2007). To measure vesicle abundance at this step, we immunostained cells for endogenous Atg12 and quantified Atg12-positive punctae. We found that

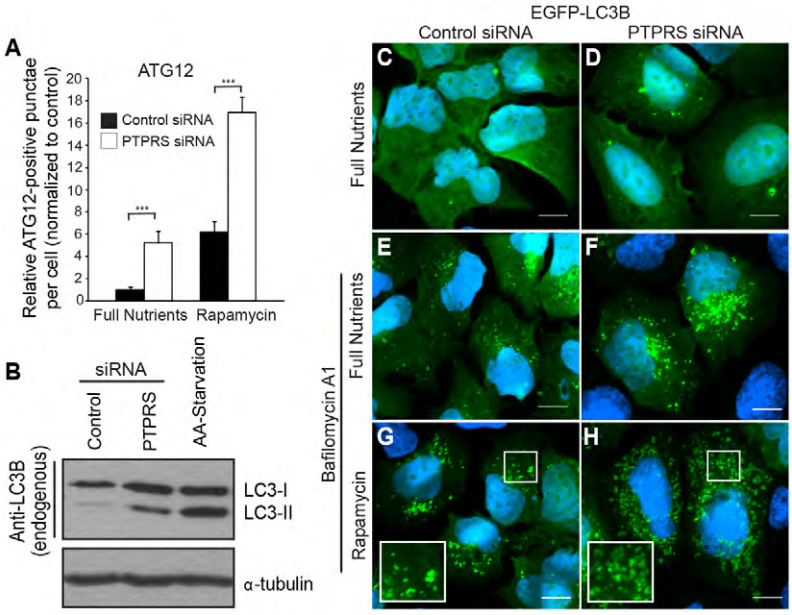

Fig. 2. Loss of PTPs hyperactivates autophagy. (**A**) ATG12-positive punctae were quantified from 60× magnification images of cells transfected with control (black) or *PTPRS* siRNAs (white) and treated for 1 hour with normal growth medium (full nutrients) or 50 nM rapamycin. Values represent relative ATG12-positive punctae per cell following normalization to control cells cultured with full nutrients. Bars represent s.e.m.; ***P<0.001. (**B**) LC3-I and LC3-II were analyzed by western blot using whole cell lysates from cells transfected with control or *PTPRS* siRNA or starved of amino acids. α-tubulin was probed as a loading control. (**C**–**H**) EGFP–LC3-positive punctae were visualized in U2OS cells transfected with control (C,E,G) or *PTPRS* (D,F,H) siRNA following treatment for 2 hours with normal growth medium (full nutrients; C,D), 100 nM bafilomycin A1 (Baf-A1; E,F), or 50 nM rapamycin and 100 nM Baf-A1 (G,H) (green, EGFP-LC3; blue, nuclei). Insets are 2× magnifications of EGFP–LC3-positive AVs. Scale bars: 10 μm.

knockdown of PTPs increased AV abundance three- or fivefold over the control when cells were cultured with rapamycin, a potent mTOR inhibitor and autophagy inducer, or full nutrients, respectively (Fig. 2A, supplementary material Fig. S2B).

The membrane-bound Atg5–Atg12–Atg16L complex permits lipidation of LC3, which is a classic marker for AVs (Hanada et al., 2007). LC3 is unique among the autophagy proteins in that a portion of it remains membrane bound and is degraded in the lysosome along with vesicle cargo. Therefore, lysosomal function can be inhibited [i.e. with bafilomycin A1 (Baf-A1) or chloroquine treatment] and LC3 accumulation used as a measure of autophagic flux (Tanida et al., 2005). We found that both knockdown of PTPs and amino acid starvation increased the abundance of LC3-II, the AV-lipidated form of LC3, when lysates were probed with endogenous antibodies (Fig. 2B). Similarly, we observed an increased number of EGFP–LC3-positive punctae when PTPs expression was reduced under normal growth conditions, and these structures accumulated substantially when cells were cultured with Baf-A1, indicating their functionality (Fig. 2C–F). Knockdown of PTPs caused an even greater increase in EGFP–LC3 punctae above the control level when cells were treated with both Baf-A1 and rapamycin (Fig. 2G,H). Similar results were obtained when AVs were quantified from cells immunostained for endogenous LC3 (supplementary material Fig. S2C).

To confirm hyperactive autophagy in the absence of PTPs independently of fluorescent markers, we detected AVs by transmission electron microscopy (TEM). AVs are hallmarked by unique double membranes and by the presence of engulfed cytosolic content: features that allow them to be easily detected by TEM. Although control cells contained very few AVs, chloroquine treatment increased their abundance, most of which appeared to be autolysosomal, as expected (Fig. 3A,B). Similarly, cells deprived of amino acids for 1 hour harbored elevated numbers of double-membrane AVs, as did cells transfected with siRNAs against PTPs, but cultured in full nutrients (Fig. 3C,D). To establish this phenotype independently of RNAi, we examined autophagy during PTPs loss using wild-type (*Ptprs*$^{+/+}$) and PTPs knockout (*Ptprs*$^{-/-}$) murine embryonic fibroblasts (MEFs). We have previously generated *Ptprs*$^{-/-}$ mice by inserting a selectable neomycin resistance gene into the D1 phosphatase (catalytic) domain. From these mice, we generated MEFs that lack both *Ptprs* transcript and protein, as measured by northern blot and western blot, respectively (Elchebly et al., 1999). TEM analysis showed that both *Ptprs*$^{+/+}$ and *Ptprs*$^{-/-}$ primary MEFs contained a basal level of AVs; however, they were twice as abundant in *Ptprs*$^{-/-}$ MEFs (Fig. 3E-G). Collectively, these results demonstrate that loss of PTPs, by RNAi and genetic deletion, increases both constitutive and induced autophagy.

PTPs localizes to PtdIns3*P*-positive vesicles and rescues the siRNA phenotype

Given the robust PtdIns3*P* response elicited by knockdown of PTPs, we hypothesized that PTPs regulates autophagy by functioning at the level of PtdIns3*P*-positive vesicles. PTPs is a bulky receptor-like PTP with an extracellular segment and two tandem cytosolic phosphatase domains (termed D1 and D2). Complex processing events have been reported for PTPs and related enzymes, including ectodomain shedding and internalization from the cell surface (Aicher et al., 1997; Ruhe et al., 2006). To determine the localization of PTPs phosphatase domains, untagged full-length protein (FL-PTPs) was transiently expressed in U2OS EGFP–2xFYVE cells and detected by fluorescent microscopy using D1-targeted monoclonal antibodies. We found that in addition to its presence at the plasma membrane, PTPs localized to the perinuclear region and to numerous intracellular-vesicle-like structures, many of which were positive for PtdIns3*P* (Fig. 4A). Strikingly, autophagy induction by amino acid starvation induced a redistribution of PTPs to smaller vesicles, which were abundant throughout the cytosol and were almost entirely PtdIns3*P* positive (Fig. 4B,C). In support of the notion that this localization was autophagic, we discovered that PTPs was also capable of localizing to mRFP–LC3-positive punctae in the context of both basal and induced autophagy (supplementary material Fig. S3B).

We further used exogenous PTPs expression in an RNAi rescue experiment to demonstrate the specificity of phenotype induced by *PTPRS* siRNA. The naturally occurring isoform of PTPs used in our studies lacks the fourth through seventh fibronectin domains

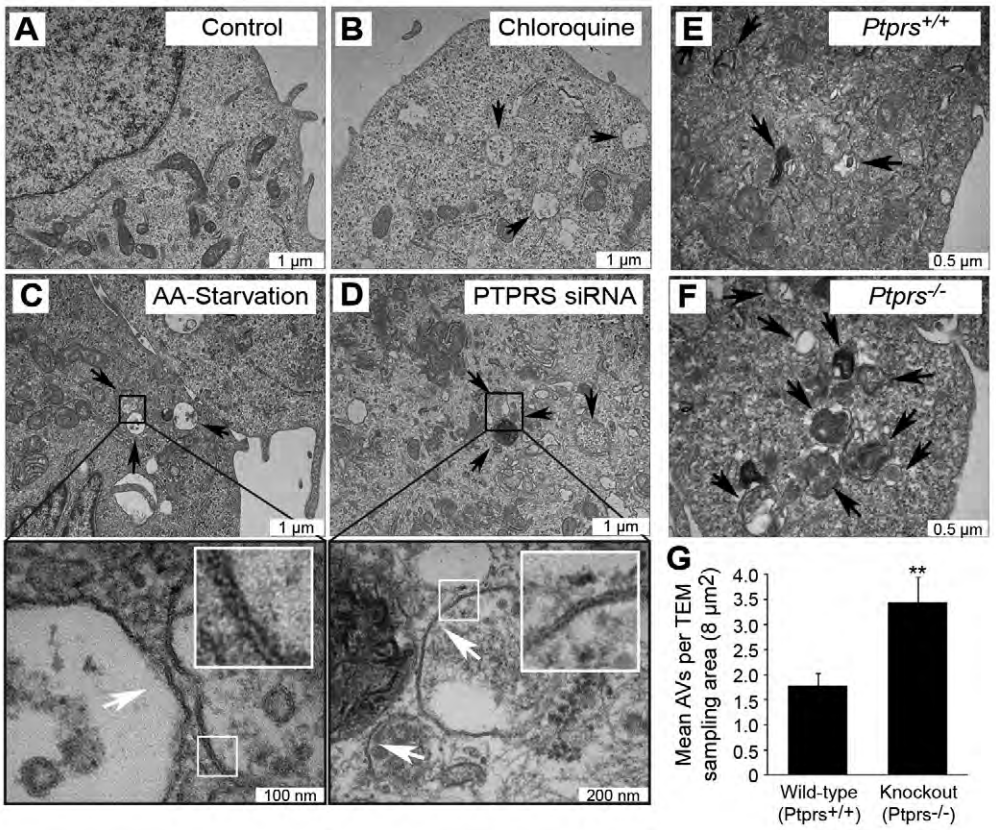

Fig. 3. Loss of PTPs increases autophagic vesicle abundance as measured by electron microscopy. (**A**–**D**) Few autophagic vesicles (AVs) were found by transmission electron microscopy (TEM) within control cells cultured in full nutrients (A), but were abundant in chloroquine-treated cells (B), amino acid (AA)-starved cells (C) and cells transfected with *PTPRS* siRNA (D). Black arrows indicate autophagic vesicles. White box insets are 3× magnifications. White arrows indicate double membranes. (**E**–**G**) Primary wild-type (*Ptprs*$^{+/+}$, E) and knockout (*Ptprs*$^{-/-}$, F) MEFs were analyzed by TEM and AVs quantified (G). AVs, defined as double-membrane structures containing cytosolic components, were counted from 8 μm^2 sampling regions per cell. Values represent mean AVs per sampling area. Bars represent s.e.m.; $^{**}P<0.01$.

(present in the longest isoform): a region encompassing the sequence targeted by a potent siRNA (siRNA-1; see supplementary material Fig. S1E,J,K) (Pulido et al., 1995). The accumulation of small, abundant, non-perinuclear PtdIns3*P*-positive vesicles induced by siRNA transfection was rescued by exogenous expression of PTPs, an effect that was dose dependent (Fig. 4D,E). This result suggests a target-specific effect of siRNA-mediated knockdown of PTPs and a role for this enzyme in PtdIns3*P* signaling.

To verify that the PTPs-positive punctate structures were in fact vesicles functioning in a lysosomal pathway, we monitored the localization of PTPs in Baf-A1-treated cells. Baf-A1 prevents maturing vesicles (e.g. endocytic and autophagic) from fusing with lysosomes and in turn, they accumulate in a perinuclear region. We found that PTPs-positive vesicular structures began to accumulate quickly (within 15 minutes) and densely populated the perinuclear region within several hours (Fig. 4F). This suggests that PTPs normally localizes to vesicles destined for the lysosome.

Finally, to determine whether PTPs functions upstream or downstream of PtdIns3*P* at the starvation-induced punctae, we analyzed its localization in cells depleted of the phospholipid. Autophagy was induced by amino acid starvation in cells treated with wortmannin, a potent and irreversible inhibitor of Vps34 and other phosphoinositide 3-kinase isoforms, or vehicle (DMSO). In vehicle-treated cells, starvation induced the formation of abundant PtdIns3*P*-positive vesicles, which also contained PTPs (Fig. 5A). Conversely, wortmannin treatment essentially ablated the formation of PtdIns3*P* during starvation; however, PTPs was still recruited to the abundant punctate structures (Fig. 5B). This finding suggests that the localization of PTPs to intracellular structures formed during autophagy occurs upstream, or independently, of PtdIns3*P*.

Discussion

Using a high-content cell-based RNAi screen, we have identified phosphatases whose knockdown elevates cellular PtdIns3*P*. Notably, RNAi-mediated knockdown of MTMR6 and several other phosphatases resulted in swollen and often perinuclear PtdIns3*P*-positive vesicles. Previous studies have shown similar phenotypes when endocytic PtdIns3*P* is elevated, for example, by constitutive activation of early endosomal Rab5, or knockdown of the phosphatidylinositol 5-kinase PIKfyve (Murray et al., 2002; Rutherford et al., 2006). Accordingly, the vesicles observed following knockdown of these phosphatases are probably endosomal, and these enzymes, including MTMR6, might function in endocytic signaling. Of note, knockdown of both PTPN11 (SHP2) and PTPN13 (PTPL1) resulted in increased numbers of EGFP–2xFYVE punctae (supplementary material Table S1). PTPN13, a phosphatase that is proposed to have both tumor suppressive and oncogenic functions, has been implicated in several signal transduction pathways. Specifically, PTPN13 was shown to inhibit PI3K/Akt signaling and thus, the PtdIns3*P* phenotype elicited by knockdown could potentially be explained by altered 3′-phosphoinositide metabolism (Abaan and Toretsky, 2008; Dromard et al., 2007). Mutations in SHP2 are associated with several human diseases, most notably Noonan syndrome, LEOPARD syndrome and juvenile myelomonocytic leukemia (Araki et al., 2004; Kontaridis et al., 2006; Mohi and Neel, 2007; Mohi et al., 2005). Its activity has been linked to numerous signaling pathways, often downstream of receptor tyrosine kinases, and the observed phenotype could be a consequence of disruption of any number of substrates (Chan et al., 2008).

Surprisingly, we did not identify MTMR3 or MTMR14 (hJumpy), the PtdIns3*P* phosphatases with reported roles in autophagy. The myotubularin phosphatases comprise a large, highly

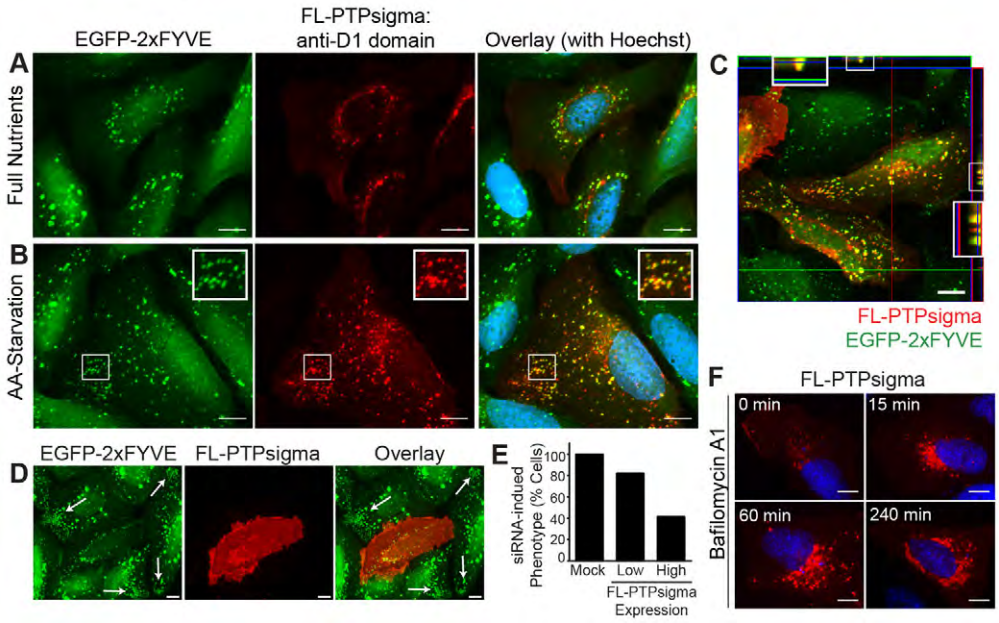

Fig. 4. Exogenous PTPs localizes to PtdIns3*P* vesicles and rescues the siRNA phenotype. (**A**,**B**) FL-PTPs was transiently expressed in U2OS EGFP–2xFYVE cells and PtdIns3*P* and PTPs imaged by fluorescent microscopy following incubation for 2 hours with full nutrient medium (A) or amino acid starvation medium (B) [green, PtdIns3*P*; red, anti-PTPs (D1-targeted antibodies); blue, nuclei]. Insets are 2× magnifications of boxed regions. Scale bars: 10 µm. (**C**) U2OS EGFP–2xFYVE cells transfected with FL-PTPs and amino acid starved for 2 hours were imaged using D1-targeted PTPs antibodies. A *Z*-stack of 0.25 µm increments was captured using sequential channel acquisition and confocal microscopy, with the third slice displayed and *Z*-stacks through the *X* and *Y* planes shown at the border. Insets are 2× magnifications of boxed regions. Scale bar: 10 µm (green, PtdIns3*P*, EGFP–2xFYVE; red, anti-PTPs; yellow, colocalization). (**D**,**E**) U2OS EGFP–2xFYVE cells were transfected with *PTPRS* siRNA-1 for 48 hours, after which FL-PTPs (which lacks the sequence targeted by siRNA-1) was introduced for an additional 24 hours. PtdIns3*P* and PTPs were imaged as previously described. The presence of siRNA-induced phenotype (abundant, non-perinuclear EGFP–2xFYVE-positive vesicles; indicated by white arrows in D) was determined for cells expressing no, low or high levels of FL-PTPs (E). Scale bars: 10 µm. (**F**) FL-PTPs-positive vesicular structures accumulate when lysosomal fusion is inhibited. U2OS cells expressing FL-PTPs for 24 hours were treated with 100 nM Baf-A1 in full nutrient medium for 0, 15, 60 or 240 minutes and FL-PTPs imaged using D1-targeted PTPs antibodies (red). Nuclei were stained with Hoechst 33342 (blue). Scale bars: 10 µm.

conserved family of enzymes whose members have been shown to function as heteromeric partners (Lorenzo et al., 2006). As one example, MTMR3 and MTMR4, both FYVE-domain containing phosphatases, have been demonstrated to interact with one another and inhibit PtdIns3*P* (Lorenzo et al., 2006). Accordingly, gene-by-gene loss-of-function analysis of this family might not reveal phenotypes if compensation within the family occurs. Furthermore, these enzymes may serve cell- or context-specific functions that are not revealed in this study.

The most striking result from this study was the presence of abundant PtdIns3*P*-positive vesicles following knockdown of PTPs, which phenocopied that of an autophagic cell. We confirmed hyperactive autophagy in the absence of PTPs through the use of several autophagy markers, as well as electron microscopy. Atg12- and LC3-positive autophagic vesicles were substantially more abundant in the absence of PTPs when cells were cultured in full nutrients (constitutive AVs) or treated with rapamycin (induced AVs). These autophagic vesicles accumulated upon treatment with

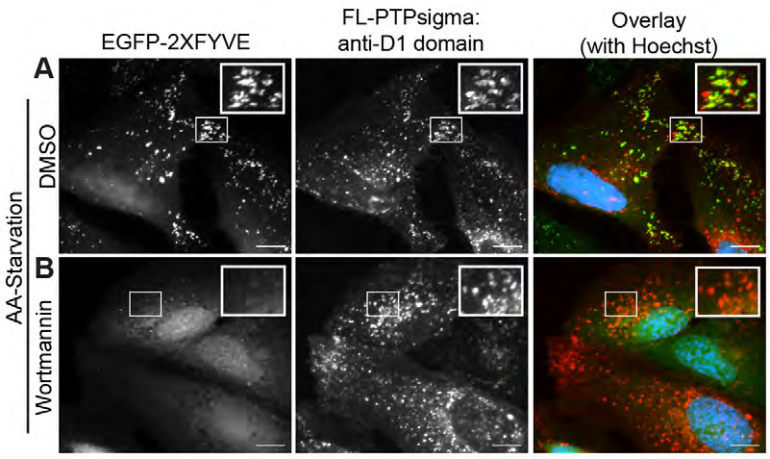

Fig. 5. Localization of PTPs to vesicular structures does not require PtdIns3*P*. (**A**,**B**) U2OS cells expressing FL-PTPs were treated with vehicle (DMSO; A) or 100 nM wortmannin (PI3K inhibitor; B) for 2 hours while cultured in amino acid starvation medium and PtdIns3*P* and PTPs was imaged by fluorescent microscopy [green, PtdIns3*P*, EGFP–2xFYVE; red, anti-PTPs (D1-targeted antibodies); blue, nuclei]. Insets are 2× magnifications of boxed regions. Scale bars: 10 µm.

the lysosomal inhibitors, Baf-A1 and chloroquine, demonstrating that they were functional and destined for lysosomal degradation. This phenotype suggests that PTPS regulates an early step in autophagy induction, and its loss results in increased autophagic vesicle generation. This is consistent with the fact that PtdIns3*P* is generated on early phagophores and is required for proper autophagic vesicle formation. A role for PTPS in autophagy induction and more specifically in PtdIns3*P* regulation, is supported by our findings that PTPS localizes to PtdIns3*P*-positive vesicles that increase in number during autophagy.

It remains to be addressed how PTPS is targeted to autophagic vesicles. PTPS is expressed at the cell surface in a two-subunit complex comprised of a large ectodomain and a membrane-spanning intracellular domain. Accordingly, it is implicated in cell–cell and cell–ECM interactions, and it is a crucial regulator of axon homeostasis and neuronal development (Aicher et al., 1997; Elchebly et al., 1999; Uetani et al., 2006; Wallace et al., 1999). Relevant to our own work, ectodomain shedding and internalization of a membrane-bound C-terminal fragment has been demonstrated previously (Aicher et al., 1997). Through immunofluorescence analysis of PTPS using D1-domain-specific antibodies, we place intracellular PTPS on PtdIns3*P*-positive autophagic vesicles. Autophagosomes frequently fuse with endosomes during their maturation, forming hybrid organelles called amphisomes, establishing the possibility that PTPS is internalized by endocytosis to arrive at autophagic vesicles (Klionsky, 2007). Furthermore, the close relative of PTPS LAR (PTPRF), undergoes an additional proteolytic event whereby a soluble intracellular domain is formed and targeted inside the cell, similarly to the Notch receptor (Ruhe et al., 2006). PTPS contains similar cleavage residues to LAR, making it therefore plausible that PTPS is targeted from the plasma membrane to autophagic vesicles through a series of proteolytic events in response to autophagic stimuli. Thus, this phosphatase might serve several unique functions during various cellular conditions that are governed by its subcellular localization.

An important finding presented here is the recruitment of PTPS to vesicular structures during amino acid starvation, which occurs even in the absence of PtdIns3*P* generation. This finding, together with the hyperactivation of autophagy elicited by knockdown of PTPS (as measured by PtdIns3*P*, Atg12 and LC3), suggests that PTPS regulates autophagy at an early step upstream of this lipid. In further support of this, we found that although almost all PTPS-positive vesicles are also positive for PtdIns3*P* (EGFP–2xFYVE presence), fewer harbored LC3, a marker that is incorporated into AVs at later stages of maturation.

There are several potential mechanisms by which PTPS might function to regulate autophagy. First, it is possible that PTPS directly dephosphorylates PtdIns3*P* following recruitment to AVs. We tested the activity of recombinant PTPS in vitro, and although we could not detect PtdIns3*P* phosphatase activity, it cannot be entirely excluded that PtdIns3*P* does not serve as a direct substrate in vivo (supplementary material Fig. S4). It is also possible that PTPS uses its robust protein phosphatase activity to regulate the function of a PtdIns3*P*-modifying enzyme, such as a PtdIns3*P* phosphatase or a phosphoinositide 4- or 5-kinase. Alternatively, PTPS could control the activity of Vps34, which contains at least one phosphotyrosine site, or another component within the larger Vps34 complex (Imami et al., 2008). Finally, PTPS might contribute to the regulation of autophagy at the earliest initiation step, which is executed by a complex of autophagy proteins, namely ULK1 (Atg1) and Atg13. The functional formation of this complex, which permits the generation of the PtdIns3*P*-positive phagophore, was recently found to be tightly regulated by phosphorylation events (Chang and Neufeld, 2009; Ganley et al., 2009; Hosokawa et al., 2009; Jung et al., 2009). The aim of future work will be to determine the precise mechanism by which PTPS functions to regulate autophagy.

Materials and Methods

siRNA screen and validation

U2OS EGFP–2xFYVE cells were seeded on 96-well plates (2000 cells per well) in McCoy's 5A medium (Invitrogen, Carlsbad, CA) supplemented with 10% fetal bovine serum (FBS, Invitrogen) at 37°C for 24 hours. Four siRNA molecules per phosphatase gene (phosphatase siRNA library version 2.0, Qiagen, Valencia, CA) were transfected per well at a final concentration of 25 nM using 0.2 µl HiPerfect transfection reagent (Qiagen) per well. After 48 hours, cells were fixed with 3.7% formaldehyde and nuclei were stained with Hoechst 33342 (Invitrogen). Cells were visualized at 40× magnification on a Zeiss LSM 510 Meta confocal microscope (Oberkochen, Germany) and EGFP–2xFYVE fluorescence was compared with that of control siRNA transfected cells within each plate. Triplicate wells from each gene were qualitatively scored by two independent scorers on a scale from –100 (decreased EGFP–2xFYVE signal and distribution) to +100 (increased) and mean scores were determined. Twenty-seven phosphatase genes whose knockdown increased EGFP–2xFYVE fluorescence in the primary screen were used in a secondary screen, where four siRNAs were individually transfected to eliminate off-target hits. The primary score was multiplied by a binned secondary screen score (score of 1.0 for 3/4 or 4/4 siRNAs yielding a phenotype; 0.75 for 2/4 siRNAs; and 0 for 0/4 or 1/4 siRNAs). Quantitative real-time PCR (qRT-PCR) assays with SYBR green dye (Roche, Basel, Switzerland) and gene-specific primers confirmed that siRNAs effectively reduced mRNA expression of target genes. For imaging, cells were cultured on number 1.5 coverglass, transfections repeated as above, cells fixed, nuclei stained, and coverglass inverted into microslides with mounting gel. A control siRNA transfected well was cultured for 3 hours in amino acid starvation medium [Dulbecco's phosphate-buffered saline (DPBS) with 10% FBS and 1 g/l D-glucose]. Cells were imaged using a 60× oil objective on a Nikon TE300 fluorescent microscope (Tokyo, Japan). EGFP–2xFYVE-positive vesicles were quantified using image analysis software.

Phospholipid labeling, extraction and thin-layer chromatography

U2OS cells were seeded in McCoy's 5A with 10% FBS at 200,000 cells per well of six-well tissue culture plates. After 24 hours, control or *PTPRS* siRNAs were transfected at a final concentration of 25 nM using 2 µl HiPerfect transfection reagent per ml medium. Control siRNA was All-star Negative Control (Qiagen) and *PTPRS* siRNAs were two unique sequences (SI02759288, SI03056284, Qiagen). After 48 hours of transfection, the medium was replaced with phosphate-free DMEM (Invitrogen) supplemented with 10% phosphate-free FBS for 30 minutes. [^{32}P]O_4 (0.25 mCi) was added per ml of medium for an additional 2 hours (Perkin Elmer, Waltham, MA). Radiolabeling was quenched with ice-cold TCA (10% final concentration) and cells incubated on ice for 1 hour. Cells were scraped, pelleted and lipids extracted via an acidified Bligh and Dyer method (Bird, 1994). Lipids were lyophilized, resuspended in chloroform:methanol (1:1), spotted on 20 cm × 20 cm silica gel TLC plates (Whatman, Maidstone, UK), and resolved in a chamber using boric acid buffer (Walsh et al., 1991). A PtdIns3*P* standard was generated by incubating synthetic phosphatidylinositol (diC16 PtdIns; Echelon, Salt Lake City, UT) with immunoprecipitated PI3K (using anti-p85, Cell Signaling, Danvers, MA) and [^{32}P]ATP (Perkin Elmer). The TLC plate was exposed to film for 20 hours at –80°C and developed.

Fluorescent microscopy and western blot analyses of autophagy markers

U2OS cells were seeded at a density of 35,000 cells per well in McCoy's 5A medium with 10% FBS on number 1.5 coverglasses in 24-well tissue culture plates (for fluorescent imaging) or 150,000 cells per well on six-well dishes (for western blot). After 24 hours, cells were transfected with control or *PTPRS* siRNAs for 48 hours, as described above. Following, cells were treated for 1–2 hours in amino acid starvation medium or with 50 nM rapamycin (Calbiochem, San Diego, CA), 25 µM chloroquine (Sigma, St Louis, MO), 100 nM Baf-A1 (A.G. Scientific, San Diego, CA) or normal growth medium (full nutrients; McCoy's 5A with 10% FBS), as indicated. For western blots, cells were lysed [in 10 mM KPO_4, 1 mM EDTA, 10 mM $MgCl_2$, 5 mM EGTA, 50 mM bis-glycerophosphate, 0.5% NP40, 0.1% Brij35, 0.1% sodium deoxycholate, 1 mM $NaVO_4$, 5 mM NaF, 2 mM DTT, and complete protease inhibitors (Sigma)] and 20 µg of total protein was resolved by SDS-PAGE. Proteins were transferred to PVDF membranes and probed with primary antibodies (LC3B, Cell Signaling Technologies; anti-α-tubulin, Sigma) for 16 hours at 4°C followed by secondary antibodies (HRP-linked rabbit or mouse IgG, GE, Piscataway, NJ) for 1 hour at room temperature. Proteins were detected by enhanced chemiluminescence. For EGFP–LC3 imaging, U2OS cells stably expressing ptfLC3 (Addgene plasmid 21074) (Kimura et al., 2007) were fixed with 3.7% formaldehyde and nuclei stained with Hoechst 33342 (2 µg/ml). Coverglasses were inverted onto

microslides using mounting gel and cells imaged using a 100× oil-immersion objective on a Nikon Eclipse Ti fluorescence microscope. For immunofluorescence, cells were fixed with 3.7% formaldehyde, permeabilized with 0.2% Triton-X 100, and blocked with 3% bovine serum albumin (BSA) in PBS. Antibodies (LC3B, ATG12, EEA1; Cell Signaling Technologies) were added for 16 hours at 4°C followed by Alexa-Fluor-488-conjugated anti-rabbit IgG (Invitrogen) for 1 hour at room temperature. Nuclei were counterstained with Hoechst 33342, coverglasses were inverted onto microslides using mounting gel and cells were imaged using 60× or 100× oil-immersion objectives on a Nikon TE300 fluorescence microscope (LC3, ATG12) or a 63× water-immersion objective on a Zeiss LSM510 Meta confocal microscope (EEA1). For quantification, punctae were counted using image analysis software after establishing an intensity threshold.

Transmission electron microscopy

U2OS cells in 10 cm dishes were transfected with control or PTPRS siRNAs for 48 hours as described above. Cells were briefly trypsinized, pelleted, rinsed and resuspended in 2% glutaraldehyde fixative (Sigma). Cell pellets were embedded in 2% agarose, postfixed in osmium tetroxide, and dehydrated with an acetone series. Samples were infiltrated and embedded in Poly/Bed 812 resin and polymerized at 60°C for 24 hours. Ultrathin sections (70 nm) were generated with a Power Tome XL (Boeckeler Instruments, Tucson, Arizona) and placed on copper grids. Cells were examined using a JEOL 100C× Transmission Electron Microscope at 100 kV (Tokyo, Japan). Autophagic structures were quantified from images encompassing approximately 8.5 μm^2 of cell area each. Electron microscopy services were performed by the Michigan State University Center for Advanced Microscopy (East Lansing, MI).

Exogenous PTPs expression and immunofluorescence

U2OS EGFP–2xFYVE cells were seeded at a density of 20,000 cells per well in McCoy's 5A medium with 10% FBS on number 1.5 coverglasses in 24-well tissue culture dishes. Full-length *PTPRS* cDNA (BC104812) was inserted into pRK7 by *Eco*RI digestion and ligation to yield FL-PTPs-pRK7 (FL-PTPs). DNA was transfected at 0.15 µg per well using 0.45 µl FuGeneHD transfection reagent (Roche, Mannheim, Germany) in 50 µl Optimem and 450 µl McCoy's 5A with 10% FBS for 24 hours. For 2 hours, cells were cultured with full nutrient medium or starved of amino acids (Fig. 4A-C), or amino acid starved while treated with DMSO or 100 nM wortmannin (Sigma) (Fig. 5, supplementary material Fig. S3). Alternatively, cells were treated with Baf-A1 (100 nM in full nutrient medium) for 0, 15, 60 or 240 minutes (Fig. 4E). Cells were then fixed with 3.7% formaldehyde, permeabilized with 0.2% Triton X-100, blocked in 3% BSA, and stained with antibodies targeting the D1 domain of PTPs for 2 hours at room temperature. AF-546-conjugated anti-mouse-IgG (Invitrogen) were incubated for an additional hour at room temperature and nuclei were stained with Hoechst 33342. Cells were imaged using oil-immersion objectives at 60× on a Nikon TE3000 or 100× on an Eclipse Ti fluorescent microscope. For Fig. 4C, cells were treated as above and imaged using a 63× water-immersion objective on a Zeiss LSM510 Meta microscope. Red (AF-546, FL-PTPs) and green (EGFP–2xFYVE, PtdIns3*P*) channels were captured with confocality through the *Z*-plane using 16 increments of 0.25 µm. Stacks through the indicated *X* and *Y* planes are shown at the border of an image of the third *Z*-plane. For supplementary material Fig. S3B, U2OS cells stably expressing mRFP–LC3 (Addgene plasmid 21075) (Kimura et al., 2007) were seeded, transfected, treated (full nutrient or amino acid starvation media for 2 hours), and stained as above. Images were captured at 100× using an oil-immersion objective on an Eclipse Ti fluorescent microscope.

Rescue of siRNA phenotype

U2OS EGFP–2xFYVE cells were seeded on number 1.5 coverglasses in 24-well dishes at 20,000 cells per well in McCoy's 5A medium with 10% FBS. 24 hours later, *PTPRS* siRNA-1 (CACGGCATCAGGCGTGCACAA; Qiagen) was transfected at a concentration of 25 nM using 1 µl oligofectamine per well per 500 µl McCoy's with 10% FBS (Invitrogen). FL-PTPs-pRK7 plasmid DNA was transfected 24 hours later at a concentration of 0.15 µg DNA per well using 0.45 µl FuGeneHD transfection reagent in 50 µl Optimem and 450 µl McCoy's 5A with 10% FBS for an additional 24 hours. Cells were fixed and immunostained as described above. Cells were imaged using a 60× oil objective on a Nikon TE300 fluorescent microscope for EGFP–2xFYVE phenotype (green) and FL-PTPs-pRK7 expression (red). FL-PTPs-pRK7 expression levels were categorized as high or low. The presence or absence of a robust PTPRS siRNA-induced EGFP–2xFYVE phenotype was determined (phenotype defined as the presence of small, abundant, non-perinuclear EGFP–2xFYVE-positive vesicles; indicated with white arrows in Fig. 4D) for 30–40 cells each of low and high FL-PTPs-expressing cells, as well as cells transfected with *PTPRS* siRNA-1 but not FL-PTPs-pRK7.

In vitro phosphatase assays

GST-tagged recombinant PTPs containing all residues C-terminal to the transmembrane domain (BC104812 cDNA; aa 883–1501) was generated in pGEXKG (Guan and Dixon, 1991). GST-tagged full-length MTMR6 (NM_004685.2) was generated in pGEXKG and GST-tagged recombinant PTP1B was purchased (Upstate, Billerica, MA). Proteins were purified from BL21 *Escherichia coli* after isopropyl b-D-1-thiogalactopyranoside (IPTG) induction and used in phosphatase assays. For PtdIns3*P* phosphatase reactions, 1 µg protein was suspended in 50 µl assay buffer (50 mM sodium acetate, 25 mM Tris-HCl, 10 mM DTT, pH 6.5) with 0, 25, 50 or 200 µM diC8-PtdIns3*P* and reactions carried out at 37°C for 25 minutes. For Tyr-*P* phosphatase assays, reactions were carried out as above using 0, 10, 25 or 100 µM Tyr-*P* peptide (TSTEPQpYQPGENL; Upstate) at 37°C for 15 minutes. Released phosphates were detected with malachite green (Upstate) and absorbance measured at 650 nm. Background levels from enzyme-only and substrate-only (Tyr-*P* or PtdIns3*P*) reactions were subtracted and absorbance converted to picomoles free phosphate released per minute using a standard curve.

We thank the Van Andel Institute Systems Biology lab for advice, analysis, and reagents. This work was supported by the Department of Defense Prostate Cancer Research Program of the Office of Congressionally Directed Medical Research Programs PC081089 to J.P.M. J.P.M. is also supported by Award Number R01CA138651 from the National Cancer Institute. Deposited in PMC for release after 12 months.

Supplementary material available online at
http://jcs.biologists.org/cgi/content/full/124/5/812/DC1

References

Abaan, O. D. and Toretsky, J. A. (2008). PTPL1: a large phosphatase with a split personality. *Cancer Metastasis Rev.* **27**, 205-214.

Aicher, B., Lerch, M. M., Muller, T., Schilling, J. and Ullrich, A. (1997). Cellular redistribution of protein tyrosine phosphatases LAR and PTPsigma by inducible proteolytic processing. *J. Cell Biol.* **138**, 681-696.

Araki, T., Mohi, M. G., Ismat, F. A., Bronson, R. T., Williams, I. R., Kutok, J. L., Yang, W., Pao, L. I., Gilliland, D. G., Epstein, J. A. et al. (2004). Mouse model of Noonan syndrome reveals cell type- and gene dosage-dependent effects of Ptpn11 mutation. *Nat. Med.* **10**, 849-857.

Axe, E. L., Walker, S. A., Manifava, M., Chandra, P., Roderick, H. L., Habermann, A., Griffiths, G. and Ktistakis, N. T. (2008). Autophagosome formation from membrane compartments enriched in phosphatidylinositol 3-phosphate and dynamically connected to the endoplasmic reticulum. *J. Cell Biol.* **182**, 685-701.

Bird, I. M. (1994). Analysis of cellular phosphoinositides and phosphoinositols by extraction and simple analytical procedures. *Methods Mol. Biol.* **27**, 227-248.

Chan, G., Kalaitzidis, D. and Neel, B. G. (2008). The tyrosine phosphatase Shp2 (PTPN11) in cancer. *Cancer Metastasis Rev.* **27**, 179-192.

Chang, Y. Y. and Neufeld, T. P. (2009). An Atg1/Atg13 complex with multiple roles in TOR-mediated autophagy regulation. *Mol. Biol. Cell* **20**, 2004-2014.

Dromard, M., Bompard, G., Glondu-Lassis, M., Puech, C., Chalbos, D. and Freiss, G. (2007). The putative tumor suppressor gene PTPN13/PTPL1 induces apoptosis through insulin receptor substrate-1 dephosphorylation. *Cancer Res.* **67**, 6806-6813.

Elchebly, M., Wagner, J., Kennedy, T. E., Lanctot, C., Michaliszyn, E., Itie, A., Drouin, J. and Tremblay, M. L. (1999). Neuroendocrine dysplasia in mice lacking protein tyrosine phosphatase sigma. *Nat. Genet.* **21**, 330-333.

Ganley, I. G., Lam du, H., Wang, J., Ding, X., Chen, S. and Jiang, X. (2009). ULK1.ATG13.FIP200 complex mediates mTOR signaling and is essential for autophagy. *J. Biol. Chem.* **284**, 12297-12305.

Gaullier, J. M., Simonsen, A., D'Arrigo, A., Bremnes, B., Stenmark, H. and Aasland, R. (1998). FYVE fingers bind PtdIns(3)P. *Nature* **394**, 432-433.

Gillooly, D. J., Morrow, I. C., Lindsay, M., Gould, R., Bryant, N. J., Gaullier, J. M., Parton, R. G. and Stenmark, H. (2000). Localization of phosphatidylinositol 3-phosphate in yeast and mammalian cells. *EMBO J.* **19**, 4577-4588.

Guan, K. L. and Dixon, J. E. (1991). Eukaryotic proteins expressed in Escherichia coli: an improved thrombin cleavage and purification procedure of fusion proteins with glutathione S-transferase. *Anal. Biochem.* **192**, 262-267.

Hanada, T., Noda, N. N., Satomi, Y., Ichimura, Y., Fujioka, Y., Takao, T., Inagaki, F. and Ohsumi, Y. (2007). The Atg12-Atg5 conjugate has a novel E3-like activity for protein lipidation in autophagy. *J. Biol. Chem.* **282**, 37298-37302.

Hosokawa, N., Hara, T., Kaizuka, T., Kishi, C., Takamura, A., Miura, Y., Iemura, S., Natsume, T., Takehana, K., Yamada, N. et al. (2009). Nutrient-dependent mTORC1 association with the ULK1-Atg13-FIP200 complex required for autophagy. *Mol. Biol. Cell* **20**, 1981-1991.

Imami, K., Sugiyama, N., Kyono, Y., Tomita, M. and Ishihama, Y. (2008). Automated phosphoproteome analysis for cultured cancer cells by two-dimensional nanoLC-MS using a calcined titania/C18 biphasic column. *Anal. Sci.* **24**, 161-166.

Itakura, E., Kishi, C., Inoue, K. and Mizushima, N. (2008). Beclin 1 forms two distinct phosphatidylinositol 3-kinase complexes with mammalian Atg14 and UVRAG. *Mol. Biol. Cell* **19**, 5360-5372.

Juhasz, G., Hill, J. H., Yan, Y., Sass, M., Baehrecke, E. H., Backer, J. M. and Neufeld, T. P. (2008). The class III PI(3)K Vps34 promotes autophagy and endocytosis but not TOR signaling in Drosophila. *J. Cell Biol.* **181**, 655-666.

Jung, C. H., Jun, C. B., Ro, S. H., Kim, Y. M., Otto, N. M., Cao, J., Kundu, M. and Kim, D. H. (2009). ULK-Atg13-FIP200 complexes mediate mTOR signaling to the autophagy machinery. *Mol. Biol. Cell* **20**, 1992-2003.

Kihara, A., Noda, T., Ishihara, N. and Ohsumi, Y. (2001). Two distinct Vps34 phosphatidylinositol 3-kinase complexes function in autophagy and carboxypeptidase Y sorting in Saccharomyces cerevisiae. *J. Cell Biol.* **152**, 519-530.

Kimura, S., Noda, T. and Yoshimori, T. (2007). Dissection of the autophagosome maturation process by a novel reporter protein, tandem fluorescent-tagged LC3. *Autophagy* **3**, 452-460.

Klionsky, D. J. (2007). Autophagy: from phenomenology to molecular understanding in less than a decade. *Nat. Rev. Mol. Cell Biol.* **8**, 931-937.

Kontaridis, M. I., Swanson, K. D., David, F. S., Barford, D. and Neel, B. G. (2006). PTPN11 (Shp2) mutations in LEOPARD syndrome have dominant negative, not activating, effects. *J. Biol. Chem.* **281**, 6785-6792.

Lorenzo, O., Urbe, S. and Clague, M. J. (2006). Systematic analysis of myotubularins: heteromeric interactions, subcellular localisation and endosome related functions. *J. Cell Sci.* **119**, 2953-2959.

Mohi, M. G. and Neel, B. G. (2007). The role of Shp2 (PTPN11) in cancer. *Curr. Opin. Genet. Dev.* **17**, 23-30.

Mohi, M. G., Williams, I. R., Dearolf, C. R., Chan, G., Kutok, J. L., Cohen, S., Morgan, K., Boulton, C., Shigematsu, H., Keilhack, H. et al. (2005). Prognostic, therapeutic, and mechanistic implications of a mouse model of leukemia evoked by Shp2 (PTPN11) mutations. *Cancer Cell* **7**, 179-191.

Murray, J. T., Panaretou, C., Stenmark, H., Miaczynska, M. and Backer, J. M. (2002). Role of Rab5 in the recruitment of hVps34/p150 to the early endosome. *Traffic* **3**, 416-427.

Obara, K., Noda, T., Niimi, K. and Ohsumi, Y. (2008a). Transport of phosphatidylinositol 3-phosphate into the vacuole via autophagic membranes in Saccharomyces cerevisiae. *Genes Cells* **13**, 537-547.

Obara, K., Sekito, T., Niimi, K. and Ohsumi, Y. (2008b). The Atg18-Atg2 complex is recruited to autophagic membranes via phosphatidylinositol 3-phosphate and exerts an essential function. *J. Biol. Chem.* **283**, 23972-23980.

Petiot, A., Ogier-Denis, E., Blommaart, E. F., Meijer, A. J. and Codogno, P. (2000). Distinct classes of phosphatidylinositol 3′-kinases are involved in signaling pathways that control macroautophagy in HT-29 cells. *J. Biol. Chem.* **275**, 992-998.

Proikas-Cezanne, T., Waddell, S., Gaugel, A., Frickey, T., Lupas, A. and Nordheim, A. (2004). WIPI-1alpha (WIPI49), a member of the novel 7-bladed WIPI protein family, is aberrantly expressed in human cancer and is linked to starvation-induced autophagy. *Oncogene* **23**, 9314-9325.

Pulido, R., Serra-Pages, C., Tang, M. and Streuli, M. (1995). The LAR/PTP delta/PTP sigma subfamily of transmembrane protein-tyrosine-phosphatases: multiple human LAR, PTP delta, and PTP sigma isoforms are expressed in a tissue-specific manner and associate with the LAR-interacting protein LIP.1. *Proc. Natl. Acad. Sci. USA* **92**, 11686-11690.

Ruhe, J. E., Streit, S., Hart, S. and Ullrich, A. (2006). EGFR signaling leads to downregulation of PTP-LAR via TACE-mediated proteolytic processing. *Cell. Signal.* **18**, 1515-1527.

Rutherford, A. C., Traer, C., Wassmer, T., Pattni, K., Bujny, M. V., Carlton, J. G., Stenmark, H. and Cullen, P. J. (2006). The mammalian phosphatidylinositol 3-phosphate 5-kinase (PIKfyve) regulates endosome-to-TGN retrograde transport. *J. Cell Sci.* **119**, 3944-3957.

Taguchi-Atarashi, N., Hamasaki, M., Matsunaga, K., Omori, H., Ktistakis, N. T., Yoshimori, T. and Noda, T. (2010). Modulation of local PtdIns3P levels by the PI phosphatase MTMR3 regulates constitutive autophagy. *Traffic* **11**, 468-478.

Tanida, I., Minematsu-Ikeguchi, N., Ueno, T. and Kominami, E. (2005). Lysosomal turnover, but not a cellular level, of endogenous LC3 is a marker for autophagy. *Autophagy* **1**, 84-91.

Uetani, N., Chagnon, M. J., Kennedy, T. E., Iwakura, Y. and Tremblay, M. L. (2006). Mammalian motoneuron axon targeting requires receptor protein tyrosine phosphatases sigma and delta. *J. Neurosci.* **26**, 5872-5880.

Vergne, I., Roberts, E., Elmaoued, R. A., Tosch, V., Delgado, M. A., Proikas-Cezanne, T., Laporte, J. and Deretic, V. (2009). Control of autophagy initiation by phosphoinositide 3-phosphatase jumpy. *EMBO J.* **28**, 2244-2258.

Wallace, M. J., Batt, J., Fladd, C. A., Henderson, J. T., Skarnes, W. and Rotin, D. (1999). Neuronal defects and posterior pituitary hypoplasia in mice lacking the receptor tyrosine phosphatase PTPsigma. *Nat. Genet.* **21**, 334-338.

Walsh, J. P., Caldwell, K. K. and Majerus, P. W. (1991). Formation of phosphatidylinositol 3-phosphate by isomerization from phosphatidylinositol 4-phosphate. *Proc. Natl. Acad. Sci. USA* **88**, 9184-9187.

Zhong, Y., Wang, Q. J., Li, X., Yan, Y., Backer, J. M., Chait, B. T., Heintz, N. and Yue, Z. (2009). Distinct regulation of autophagic activity by Atg14L and Rubicon associated with Beclin 1-phosphatidylinositol-3-kinase complex. *Nat. Cell Biol.* **11**, 468-476.

Supplementary Material, Figure 1 (MacKeigan)

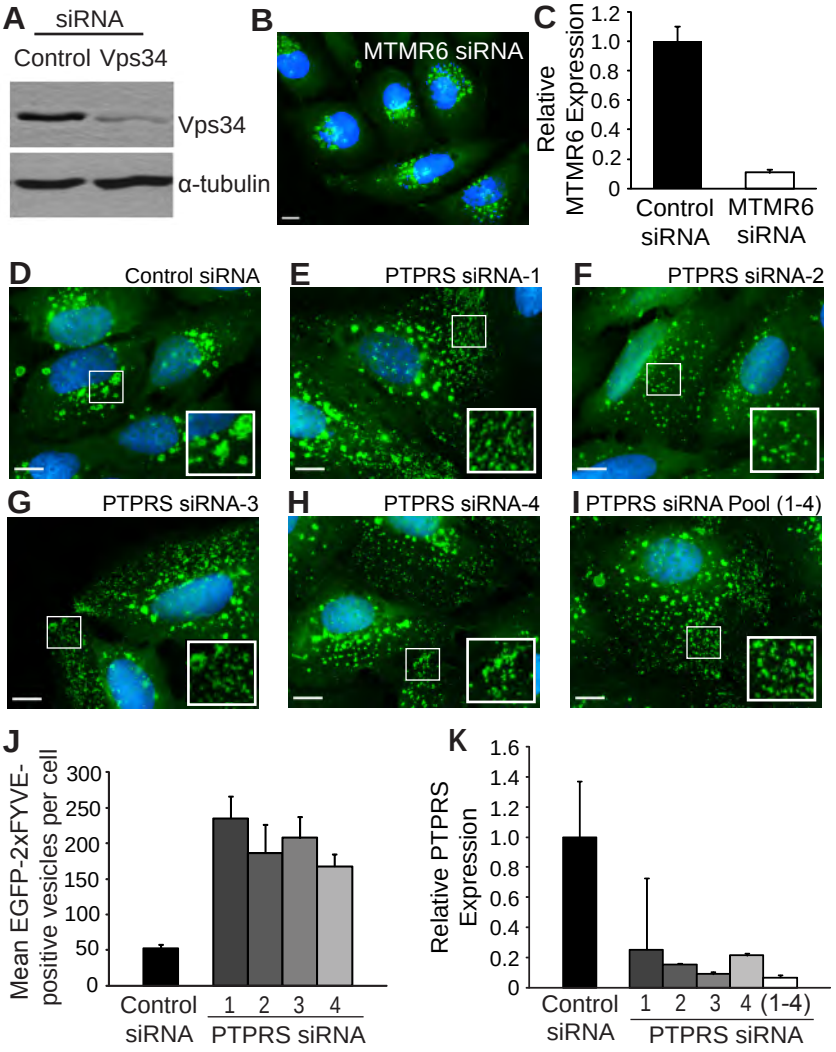

Supplementary Material, Figure 1 Continued (MacKeigan)

Fig. S1. Target genes are effectively knocked down by siRNA. (**A**) Western blot analysis of whole cell extracts following transfection with control or VPS34 siRNA shows depletion of VPS34 protein levels. α-tubulin was probed as a loading control. (**B**) U2OS-EGFP-2xFYVE cells were transfected with MTMR6 siRNA, fixed, and imaged at 60x by fluorescent microscopy as in Fig. 1. A bar, 10 μm. (C) MTMR6 mRNA was depleted by 96% following transfection with MTMR6 siRNA for 48 hours. RNA extracted from control- or MTMR6- siRNA transfected cells was converted to cDNA and MTMR6 levels determined by qRT-PCR using gene-specific primers. Values were normalized to GAPDH. (**D-I**) U2OS-EGFP-2xFYVE cells were transfected with control (D) or PTPRS siRNA [E, siRNA-1, F, siRNA-2, G, siRNA-3, H, siRNA-4, I, siRNA-pool (1-4)] for 48 hours, fixed, and imaged by fluorescent microscopy (green: PI(3)P, EGFP-2xFYVE; blue: nuclei). Insets are 2x magnifications of boxed regions, highlighting the abundant vesicles caused by PTPRS siRNA transfection. Bars, 10 μm. (**J**) EGFP-2xFYVE punctae were quantified from cells following PTPRS knockdown with four unique siRNAs. Values represent means and bars represent s.e.m. (**K**) PTPRS mRNA knockdown following 48 hour transfection with four unique siRNAs (individually or pooled) was determined by qRT-PCR using gene-specific primers and GAPDH normalization, as described above.

Supplementary Material, Figure 2 (MacKeigan)

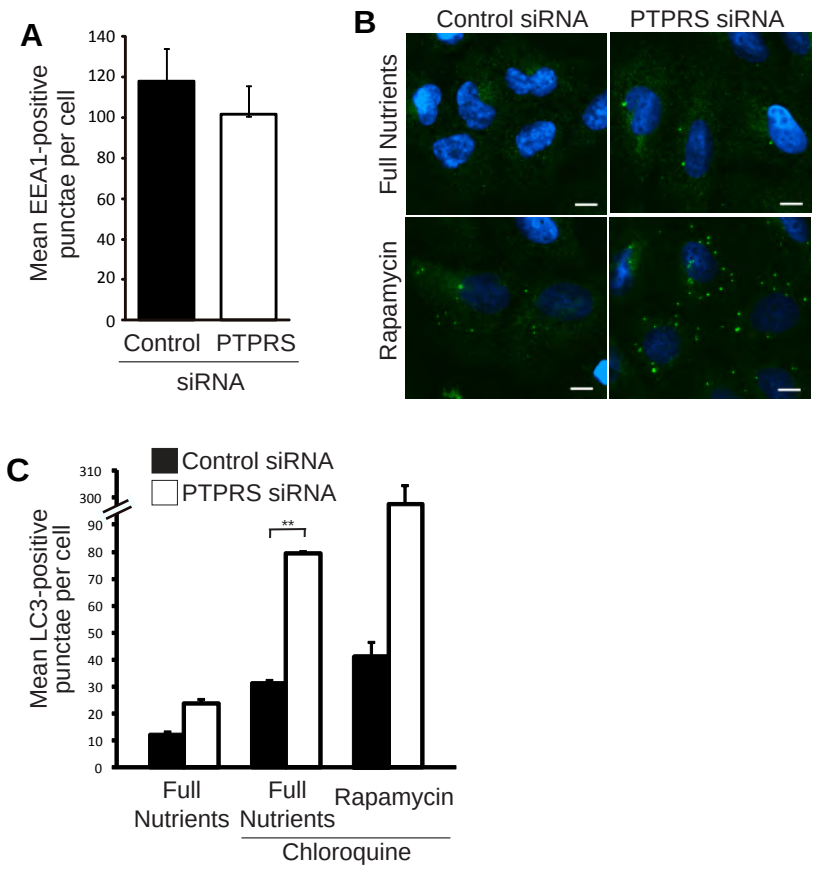

Fig. S2. PTPsigma knockdown increases the abundance of autophagic, but not endocytic, vesicles. (**A**) U2OS cells were transfected with control or PTPRS siRNAs, fixed, and immunostained with anti-EEA1 antibodies (see Fig. 1H). EEA1-positive vesicles were quantified using image analysis software. Bars represent s.e.m. (**B**) U2OS cells transfected with control (left panels) or PTPRS (right panels) siRNAs were cultured for 1 hour with nutrient-rich medium (top panels) or 50 nM rapamycin (bottom panels). Cells were stained with anti-ATG12 antibodies and imaged by fluorescent microscopy at 60x (green: ATG12; blue: nuclei). Bars, 10 µm. (**C**) U2OS cells transfected with control or PTPRS siRNAs were cultured for 1 hour with normal growth media (full nutrients; left), 25 µM chloroquine in normal growth media (middle), or 50 nM rapamycin and 25 µM chloroquine in normal growth media (right). Cells were fixed, immunostained with anti-LC3B antibodies, and imaged by fluorescent microscopy at 60x. LC3-positive punctae were quantified images using image analysis software (black: control siRNA; white: PTPRS siRNAs). Bars represent s.e.m., *$p < 0.05$, **$p < 0.01$.

Supplementary Material, Figure 3 (MacKeigan)

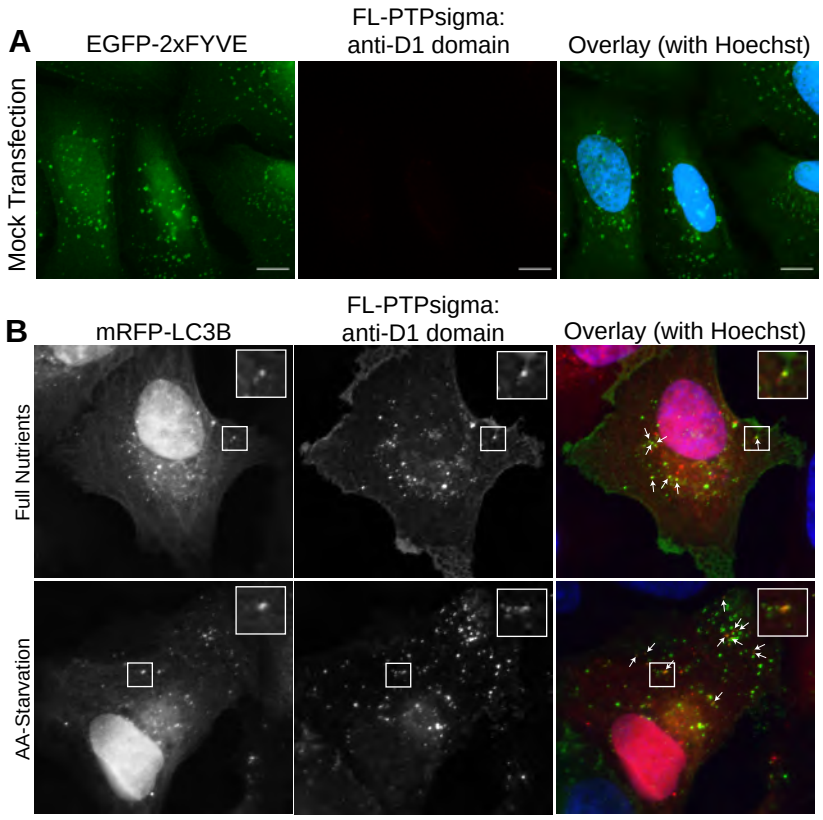

Fig. S3. FL-PTPsigma colocalization with mRFP-LC3 and mock control for FL-PTPsigma immunofluorescence. (**A**) U2OS-EGFP-2xFYVE cells were mock transfected (with transfection reagent but no DNA) for 24 hours, stained with PTPsigma (anti-D1) antibodies, and imaged as in Fig. 4A-C, Fig. 5, and (B). Absence of signal in the red channel demonstrates specificity of FL-PTPsigma expression captured in the above figures [green: PI(3)P; red: anti-PTPsigma (D1-targeted antibodies); blue: nuclei]. Bars, 10 µm. (**B**) FL-PTPsigma was transiently expressed in U2OS-mRFP-LC3 cells and LC3 and PTPsigma imaged by fluorescent microscopy following 2 hour incubation with full nutrient media (top panels) or amino acid-starvation media (lower panels) [red: mRFP-LC3; green: PTPsigma (D1-targeted antibodies); blue: nuclei]. Insets are 2x magnifications of boxed regions. White arrows indicated punctae positive for both PTPsigma and LC3.

Supplementary Material, Figure 4 (MacKeigan)

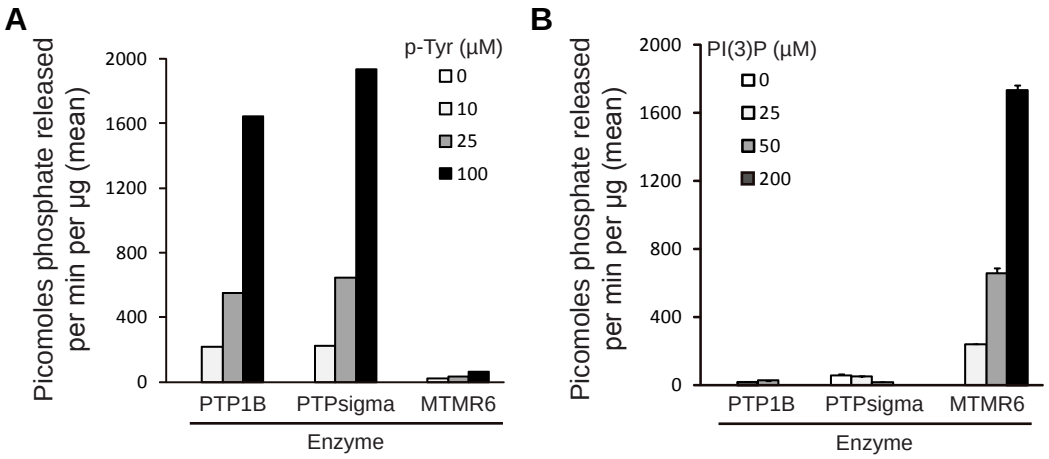

Fig. S4. PTPsigma dephosphorylates phosphotyrosine, but not PI(3)P, in vitro. (**A**) Recombinant GST-fusions of PTP1B (left), PTPsigma (middle) and MTMR6 (right) were incubated with a phosphotyrosine peptide at the indicated concentrations for 15 minutes at 37°C and released phosphates measured by malachite green quenching and 650 nm absorbance. (**B**) Recombinant GST-fusions of PTP1B (left), PTPsigma (middle) and MTMR6 (right) were incubated with water-soluble PI(3)P substrate at the indicated concentrations and released phosphates measured by malachite green quenching and 650 nm absorbance. Bars represent s.d.m.

Gene Symbol	Description	Score	Rank	siRNA sequence 1	siRNA sequence 2	siRNA sequence 3	siRNA sequence 4
ACP1	acid phosphatase 1, soluble	25	40	CCCATAGTGCACACTTGTATA	TCCGTAGGAGCTCACAGTCTA	TCGGTGTGTAATCACGTTCCA	ATGGATGAAAGCAATCTGAGA
ACP2	acid phosphatase 2, lysosomal	-17	176	CAGCCTGAAGTCTTCGGCAAA	CTGGATGTCTACAATGGTGAA	ACCAGTGAAGACATATCCCAA	CAGCGCTATCACGGCTTCCTA
ACP5	acid phosphatase 5, tartrate res	25	41	CTCGGGCAAGTCCCTCTTTAA	CTGGTACGTGCTAGCCGGAAA	ACGGCGCTGCTCATCCTGCAA	CACTGGTGTGCAAGACATCAA
ACP6	acid phosphatase 6, lysophospl	-8	167	CCATGTCAGTTTATACCTTAA	CCCGCTGGACATGTTCTTGAA	GTGCCTTTATACAATGCCAAA	GAGGCCAAACTTGAAATACAA
ACPP	acid phosphatase, prostate	42	20	ACAGATGGCGCTAGATGTTTA	CCGGACTTTGATGAGTGCTAT	CTCTATTACCATTATGGATAA	ATGAACAGGTTTATATTCGAA
ACPT	acid phosphatase, testicular	0	117	CCCGCCAAAGATGGAGGGAAT	CTGGTGTTCGTGGCTCTGGTA	CTGCTGAATGCTATCCTTGCA	CAGGGCATGGAAGGTTCTGGA
ALPI	alkaline phosphatase, intestinal	58	9	CACGTCCATCCTGTACGGCAA	TCCATTCTCCTAGGAGACAAA	CCAGACAATAAAGGGACCAAA	CCGGGCTACGTGTTCAACTCA
ALPL	alkaline phosphatase, liver/bon	25	42	CAGGATTGGAACATCAGTTAA	CCGGGACTGGTACTCAGACAA	CAGACTGCAGACATTCTCAAA	CACCATGATTTCACCATTCTT
ALPPL2	alkaline phosphatase, placental	17	63	CTGGGAAACACAAAGCAATAA	TTGCTTTATCTTGCTCTTGAA	ATCGACCATGGTCATCATGAA	CACGGTCCTCCTATACGGAAA
CDC25A	cell division cycle 25A	17	64	AAGGCGCTATTTGGCGCTTCA	AAGGGTTATCTCTTTCATACA	CAGCTTAGCTAGCATTACTAA	CTGGCCAAATAGCAAAGACAA
CDC25B	cell division cycle 25B	50	13	CAGGAGGCTGAGGAACCTAAA	CCCAGTCTGTTGAGTTAGTTA	CGCCGAGAGCTTCCTACTGAA	TTGGGTTAATACCAGCTTAAA
CDC25C	cell division cycle 25C	17	65	CAGGAAGGGCTTATGTTTAAA	CCAGAGCTATATATCCTTAAA	CCAGGGAGCCTTAAACTTATA	GAGCTGCAATCTAGTTAACTA
CDKN3	cyclin-dependent kinase inhibitc	25	43	CACAATCAAGATCTGTATCAA	TCGGGACAAATTAGCTGCACA	CACCAGTGTTATCAACTTGAA	CTAGCATAATTTGTATTGAAA
CTDP1	CTD (carboxy-terminal domain,	0	118	CCGGCTGTACGCACACACCAT	CTCCATGGTTTGCATTATTGA	CCCGACAAACTTCCCGATAGA	CCGAATATTATCAAGGGATGA
CTDSP2	CTD (carboxy-terminal domain,	8	85	CCCGGAAACAGCGGGAAGTAA	TACGATCAGCGTGACAGAGTA	CCACCTAGCCATAGTCTCAAA	CTGCGTATAAGGAGGAAGCAA
CTDSPL	CTD (carboxy-terminal domain,	8	86	CCAGTGCAACGTCAGCTTAAA	TACGCCCAACTCTTTAGCCAA	TAGGAAATGCTACATGCGGAA	TTCGTTTAAGCCTATTAGTAA
DKFZP566K0524	DKFZP566K0524 protein	17	66	CCCACCCTAACACTTAACATA	CTGGTGACAAGCTATACCTAA	TTGAATTGGTTGAATAATTAA	TCACCTCTGTTGAAACATTTA
DOLPP1	dolichyl pyrophosphate phosphá	0	119	AAGAATGCACCAAACAAACAA	CAGGGTCTACCTGCTGTACCA	GAGGTGGTTTGATTTAAGAAA	CAGGATGGACAGGATGACAGA
DUSP10	dual specificity phosphatase 10	8	87	ATGAGAATACAGGCTCTCTAA	CAGGTTCATAGACCGAAGATA	CAGGGCAGCTTAAGTGGTCTA	CCGAAGATACTACACACTTTA
DUSP11	dual specificity phosphatase 11	8	88	CAGAAACTGTTCCTTACTTAA	CCCTTATGTATTCAAGCTTAA	CACAATAAGCCTGTTAAACAA	ATGATGCAATTGAATTATTCA
DUSP12	dual specificity phosphatase 12	0	120	ATGCTTTACATGGCAATCAAA	TACCGTTTCACAAGGATTGAA	CTCAATGTACATCTTATTTCA	CAAGCTCAATGTACATCTTAT
DUSP13	dual specificity phosphatase 13	42	21	ACCCTGAGATGTAAACAGCAA	TCAGTCCATCTCTATAATAAA	ACCCAATTCAGAGATTCTTTA	CAGGTGGACACAGGTGCCAAA
DUSP14	dual specificity phosphatase 14	8	89	AAGGGAATGCATACATTGCTA	ACCCTTATTATTTAGCTGTTA	CCCAGGATTATATTAGCATTA	TAGCTGTTAAGTAACTATAAT
DUSP15	dual specificity phosphatase-lik	-42	198	ACGGGCCTGGAGGGTATTAAA	CACCACGATTGTGACAGCGTA	CTGGAGGGTATTAAAGAGACA	CCGAAATAAGATCACACACAT
DUSP16	dual specificity phosphatase 16	0	121	AAGGTTGTAGTTTACGATCAA	CCGGCCATTTGTGGAATACAA	CAGGACAAAGTGTTAATTACA	AACCCAGTTGTTACTCTCTTA
DUSP18	dual specificity phosphatase 18	33	29	ACGGGTCTCTCTCCCGAAGAA	CCAGATCACCATGGTCATCAA	CAGGAATGAATCTGCTACAAT	CAAGCTCATGCTGTCTAGCAA
DUSP19	dual specificity phosphatase 19	-8	168	ATGGTCAGTATCACTGGATAA	CAGAGTTAACCTAATGAGTCA	TACGGTCCTCTTTCTCACATA	AAGGTCATATATACTATACAA
DUSP2	dual specificity phosphatase 2	33	30	CAGCCTGAGAGCTCCAAGGAA	CTGGTCCACCACCATGTTGAA	AAACTTAGCACTTTATATTTA	CGCGGGAAAGACCGAAAGGAA
DUSP21	dual specificity phosphatase 21	0	122	AACGTAGTAAGCCTTACCTTA	TCGGTGGAAGTGGTCAACGTA	ACCGGATGGTGCCTTGTTAAA	ACGTACGATGATATCAATGTA
DUSP22	dual specificity phosphatase 22	0	123	CATGTTTATGTTGAGAACTAA	GGGCAACTTAGCCAAGTTTAA	AAGCAACATAGAGTTTAAGTA	AAGCATGAGGTCCATCAGTAT
DUSP23	dual specificity phosphatase 23	0	124	CAGTTCTACCAGCGAACGAAA	GAAGTGGACTAAAGTATTAAA	TTGGCTGAAGACACTGAAGTA	CAGGAGATGCCATTGCTGAAA
DUSP24	dual specificity phosphatase 24	-33	193	AAGCTTCTGCACATCCGGATA	CAAGATTCAGAAGGACTTGAA	CACCCTGGAGATACTCTTAAA	CTGCCTGAAAGTCTCATGTTA
DUSP3	dual specificity phosphatase 3 (	-33	194	CCCGCGGATCTACGTGGGCAA	CCGTATTTACTTAACAAGATT	AACAGATTCGTTGGAAGCTTA	TACGTTATTGTTATTATGGAA
DUSP6	dual specificity phosphatase 6	25	44	CTGCATTGCGAGACCAATCTA	TACGGACACTATTATCACTAA	TGCGGAATTGGTTAATACTAA	TCAGCTGTGCTAAACAGTATA
DUSP7	dual specificity phosphatase 7	33	31	CAAGGTGGTTTCAACAAGTTT	CGGCGGCGAGTTCACCTACAA	TACGACTTTGTCAAGAGGAAA	GAAGATGAACCTGTCACTCAA
DUSP8	dual specificity phosphatase 8	42	22	CCGCTCCTTCGTGGAGTACAA	TCCATCGAGTTCATCGATAAA	CAGGCCCGTTATAAATGTATA	GCGGGTGGTCCTCGAGCTCTA
DUT	dUTP pyrophosphatase	42	23	AAGCCTTGGATGACACCGAAA	TCCCTTCTCTTCACTAGTCTA	AAGCCTGTATTTAACTCATAT	AAAGCCTGTATTTAACTCATA
ENPP1	ectonucleotide pyrophosphatas	0	125	CACCGGCTCCTAATAACGGAA	CAGATAAATACTATTCATTTA	TGGGCAAACAGTAGACTTATA	AAGCATGAAACTTTACCCTAT
ENPP2	ectonucleotide pyrophosphatas	-33	195	ATGGATCATTATGCTGCGGAA	CGGACTAGATATGATATCTTA	AAGCCTTATAAACCAATCTTA	CAGATATATTTAAGCCTTATA
ENPP3	ectonucleotide pyrophosphatas	0	126	AACCTAATGTGTGATCTTCTA	CTGGCTGTTAGGAGTAAATCA	TAGCAATTTGGTACCTATGTA	ATGGTTATAACAATGAGTTTA
FBP1	fructose-1,6-bisphosphatase 1	0	127	CTCGCTCTGCACAGCAGTCAA	TTCCTAGAGAGCAGAAATAAA	CCTGGTTATGAACATGTTAAA	CTCCAACGACCTGGTTATGAA
FBP2	fructose-1,6-bisphosphatase 2	0	128	AGGACCCTAAATGAACGATAA	CAGGTTATGCGCTGTACGGTA	TCCACTTAATCACATACAGAA	CTCAATGCTGACGGCCATCAA
FLJ32332	likely ortholog of mouse protein	-17	177	CAGAGTGACTTTACAACTTAA	CCCAGAGACTCGGATTATCAA	CAGGATCTTGAACAGCCCAAA	TCGGATTATCAATGCAGAGAA

G6PC	glucose-6-phosphatase, catalyt	0	129	CAGCAGGTGTATACTACGTGA	TGGGATCCAGTCAACACATTA	CTGGCTTATTCCCATGTGTGA	TAGCAGAGCAATCACCACCAA
G6PC2	glucose-6-phosphatase, catalyt	50	14	CAGAGTATTCATAGCAACACA	CTGGTGGGTCCAAGAAACTCA	TGGTTAAATCTTATATTTAAA	TTGGTTAAATCTTATATTTAA
G6PC3	glucose 6 phosphatase, catalyti	0	130	CAGGTGCTGGCTGGCCTAATA	GTGGCTCAACCTCATCTTCAA	CACATGTTCAGTGCCCAGGAA	CTGGGAAATGGCCAGAAGATA
ILKAP	integrin-linked kinase-associate	0	131	ATGGAGGAATTCGAGCCTCAA	CCCGCTAGCAGTGGCGATTCA	TCGGGCAATCTTGTGTCGTTA	TTCGGTGATCTTTGGTCTGAA
IMPA1	inositol(myo)-1(or 4)-monophos	-17	178	ACGAAGAGTAATTGCTGCAAA	CCGGAAGAGACGAGTGCGGTA	TAGAAAGTTAACTGTTTGGAA	CCAGATTTGGTGACTCATCAA
INPP1	inositol polyphosphate-1-phosp	50	15	CCGTAATTAGTACAAGTGAAA	TAGATTCAACTTATCAGTATA	CTGATGGGAGTCATCAATCAA	CACCAGCAGCTGCAACTGAAA
INPP4B	inositol polyphosphate-4-phosp	8	90	AACGATTTGCCGCAAACTGAA	CCCGGAAAGTGTGAGCGGAAA	ATCGATGTCAGTGACACTTGA	CTCCATAGATTTGAAACAGAA
INPP5A	inositol polyphosphate-5-phosp	8	91	CGGAAGGTTATGCTCCAGTTA	TCGAGTGATGCGATGAAAGAA	AACAATAATATCATGGGAGAA	CGAGTGCAAATGGTCAAGAAA
INPP5B	inositol polyphosphate-5-phosp	33	32	TTGCGGGAACATACAATGTAA	AAGAAGAGGATTACACCTATA	GAGGGCAATACAGGCATTTAA	CTGCGAGATACAATTGTGAAA
INPP5D	inositol polyphosphate-5-phosp	0	132	CAGGTGCTATGCCACATTGAA	TCCCATCAACATGGTGTCCAA	CCCGGGACTGTTGACAGCCAA	TCGGAATTGCGTTTACACTTA
INPP5E	inositol polyphosphate-5-phosp	0	133	ACGCATCGTGTCTCAGATCAA	ACGGATTTCGAAGGAGATTCA	CACGTACGACAGCACCTCCAA	CAGAAATGTGCCCGACACCAA
INPP5F	inositol polyphosphate-5-phosp	50	18	AAGACCTTTACGCATATTAAA	CAGATCTTCCATGGTGGCTTA	CTGAAATAATGTGTTTCTGAA	TACCATCTCCTGATGACTCAA
ITPA	inosine triphosphatase (nucleos	8	92	CTGGAGAAGTTAAAGCCTGAA	CTGGATGAGACTTGTTTCCAA	GAGGAGGTCGTTCAGATTCTA	CAGGAGGCAGTTCGCCAGGTA
LHPP	phospholysine phosphohistidine	8	93	CAGGAGGAAACTAACAGTTCA	CCCAGTCACCTTTGCAGACAA	CCCGGTGTGTGCAGGAGGAAA	ACCACTCACCATGGGCCTTTA
LOC387870	similar to protein tyrosine phosp	0	134	TAGCAGAAAGAGGAACTTTAA	CACGATATGTTTGTCTTGGAA	CCAGGTGGTATTGTTAAAGTA	CAGGATCGTGTTCACAAGGAT
LOC389772	similar to Osteotesticular phosp	0	135	TACATTCTAGTAAGCATCTTA	TAGTTTAAATATATACAATAA	AAAGCAATATGTAAATCTTAA	AACATTATGTTGTATAGTTTA
LOC391025	similar to protein tyrosine phosp	56	12	CTCATTAATTATGATTATTGA	CAAAGGATTCCGGAACAGAAA	CAGGAGGGTCCTGTTGGCTCA	CAGATGAGTCTCAGCACAAAT
LOC400927	similar to TPTE and PTEN hom	17	67	TCCAGGTGATCTGAACCTGAA	ATGGATGTTCTTCTTCGAGTA	TCCACAGACAAACGAATTTAA	CTGGTGTCACCTATCAGTAAA
LOC442428	similar to fructose-1,6-bisphosp	25	45	CAACATTGTGACCATAGTTTA	CAAGATTAGTAAGAAAGGAAA	CAGCCTTATGGACTCTCTCAA	CACCTGGATGCTACCAGGCTA
LOC474338	SUMO1 pseudogene 3	-8	169	CAGGCTTGTGGTGATAAATAA	AAGGAAGGTGAATATATTAAA	CTCATTATTCATTATTGTTTA	CAGAGAATTGCTGATAATCAT
LPPR2	lipid phosphate phosphatase-re	0	136	CCCGTGTCTAAGCATGTGCAA	CCGGGACAACTTCAGCCCTTA	CTGCGTTGTGCATAACTTTCA	CCGCGTGGCCGAGTACCGAAA
MINPP1	multiple inositol polyphosphate	-42	199	CACGGTCAAACAGATCCGCAA	CCGAGTGCAGATGTTATTAAA	AAGTCGGAAAGTACAATGAAA	ATGAAATTCTTCCTACTTATA
M-RIP	myosin phosphatase-Rho intera	25	46	AAGCGGGACTTCACCAATGAA	CCGGACCAACAAGCAGAATCA	CGGGAGCTAGAGAAACTTCGA	GCGACGGTTCTTCATCCTTTA
MTM1	myotubularin 1	25	47	CGAATAGGTCATGGTGATAAA	TCGGTATGAGTGGGAAACGAA	GACATTGTTTATCCTAATGTA	CGGTATGAGTGGGAAACGAAA
MTMR2	myotubularin related protein 2	25	48	AACGATATGAACTTTGTGATA	CTGAGGGAGTCTAACAAGTTA	ACCACTGCAATTCACATTATA	TAGGATGAGTTTAGAACTGTA
MTMR3	myotubularin related protein 3	0	137	GACCCTTATTACCGAACCATA	TTGCCTTTAGCCGAATGTAAA	CAGCCTTAAATCAAGAATATT	AGCATGTAACTTCAAGGTTTA
MTMR4	myotubularin related protein 4	17	68	TCGGCACTGGAGAGTACCAAA	TTGCCATAGATGTAACCTAAA	AAGAGTGGCTCTCACGGCTAA	CCGGCTGCATATCAAATTCAA
MTMR6	myotubularin related protein 6	33	33	CCCGGATAGCAAGCAAACCAA	CCCGTAAATGATGCTCTTCGA	TACAAAGTTACTGTTTAACAA	AAGGGAAGTACAGATAGTTTA
MTMR8	myotubularin related protein 8	8	94	CAGCCCAAGCAGAGTATGCTA	CGGGAAGATCTAAGAGTCTAT	GGGAATTACTTTACTGATTAA	TGCCATGAGGTTTATATTTCA
MTMR9	myotubularin related protein 9	8	95	CAGACCTAGTATTCTAAGTTA	CAGGTCTAAGGATTAACTATA	ATGCCTGAACCTGTTATCTAA	TACGTTGGAATAGATCCTCTA
PDP2	pyruvate dehydrogenase phosp	8	96	CAGGACGATCATCATGGAGGA	TAGACAGGACAGGTTAATTTA	CAGGAATTAGACCATATTTAG	CCCATCCTATTGTCAAGGTTA
PDPR	pyruvate dehydrogenase phosp	58	10	ACCACATAGCCCAGTGATTAA	ATCTCTTATCTCCTTGATATA	TAGCTACAAGATTCAGCTTTA	TTGGAGCAAGTATGTACTTAA
PHOSPHO1	phosphatase, orphan 1	-8	170	CGCCAACATGTGCAAGCACAA	TCGGGTCCGGACAGCCAGTAA	TACAACTATAAAGGAGGTGAA	CCGTCCCTATCTATTCAGTTA
PHPT1	phosphohistidine phosphatase	17	69	CACGCCATTTCAACTGAGAAA	TCGGGCGACATGCAGAAGCAA	CCGATTCCACGTTTCCTTTAA	TAGCCTGGCCACAGAATTAAA
PIB5PA	phosphatidylinositol (4,5) bisph	25	49	CAGGTAACATTCAGTGAGGAA	CTGGGACTGGATCGGCTTATA	CTGGAGGTCATCCATTAGGAA	ATGGGAATACCTACCAGGTAA
PIP3AP	phosphatidylinositol-3-phosphat	0	138	CAGGGTCATGGCATACCAATA	TGGGATGTGGATTATGCTTAA	CCGGCACTCCGTTAGAATAAA	CCCGGCACTCCGTTAGAATAA
PLIP	PTEN-like phosphatase	17	70	CAGCTGCGGCTCAGCACAGTA	CACCTTGGACAACCTCCAGAA	AACCTCCAGAAGGGAGTCCAA	CAGGAGTGGAAGAGACTAGGA
PME-1	protein phosphatase methyleste	33	34	AACATCGAGCTCTGTTGTAAA	AGGCGATACATCTGAGTTCAA	AGGAAGGAAGTGAGTCTATAA	ACGGCAGCGATTATTAGTAGA
PNKP	polynucleotide kinase 3'-phosph	17	71	CACGTGAACAGGGACACGCTA	CACGTGTGAGACAGCCCTGAA	CGGGAAGTCCACCTTTCTCAA	CAAGCTGGTGATCTTCACCAA
PPAP2A	phosphatidic acid phosphatase	8	97	AACCCTGTCTGTTTACTGTAA	CTGACATTGCCAAGTATTCAA	CATGCTGTTTGTGGCACTTTA	CCGGGCAGAGACCATGTTTGA
PPAP2B	phosphatidic acid phosphatase	8	98	AGCGATCGTCCCGGAGAGCAA	CAGCACAATTTCAGAAGAAAT	CCGGATCTATTACCTGAAGAA	CCGGGCACTTGCATACTCTTA
PPAP2C	phosphatidic acid phosphatase	8	99	CCGGGTCAACTGCTCGGTCTA	TCGCTCGGACTTCAACAACTA	ACCCGCGTGTCTGATTACAAA	CATGGTGTTCTTGGCGCTGTA
PPEF1	protein phosphatase, EF hand (	17	72	CAGCATTAGTACCTACATATT	CCCAATCGGTACAATCGTTGA	ATCGAATATGCTGATGAACAA	CTGGGAAACCCTCTTCAATAA
PPEF2	protein phosphatase, EF hand (	8	100	CACATGAATATCGACATTACA	CTGCAGGAGCATTGCGCTTAA	CCCACAAGCTACAAATGCTAA	CGGAGCATTGATTTCAACAAA
PPFIA1	protein tyrosine phosphatase, r	0	139	AACGGCCTATTTAATATGTTA	CACGAGGTTGGTCATGAAAGA	CTGGTGTTTCCGAGACGGATA	TTCCAAGGTACAAACTCTTAA

PPFIA2	protein tyrosine phosphatase, r	0	140	AACGTTTGGGTGACTCATGAA	TACCAGCTGGATTTAGGTTAA	TCCAATGAACGCCTACAACTA	ACCGATGAAACTAGTCAAATA
PPFIA3	protein tyrosine phosphatase, r	25	50	ACGGCTCAACTATGACCGGAA	CACGGGTAAAGAGAACTGTTT	TCGAATGTTAGATCACCTTAA	CTGGTGGACGCTCGAATGTTA
PPFIA4	protein tyrosine phosphatase, r	25	51	CAGGATAGCTGGGTCCATTCA	TGGGTGTGTACGTACCAATAA	CAGGGACTCAGTCCAGATTAT	TCCCTGGGTAATGGATGGTAA
PPM1A	protein phosphatase 1A (forme	-58	204	AAGCGTGATTTCAAACCATAA	TTCCATGAGTATTGCAGGTAA	CAAACCATAATTCGTGTTGTA	TAAGCGTGATTTCAAACCATA
PPM1B	protein phosphatase 1B (forme	17	73	CACCTAAGCATATCTACTTTA	CGAGATAACATGAGTATTGTA	CAACCAAGTGTTTAGAATGAA	TAGCCTAACTACACACATCAA
PPM1D	protein phosphatase 1D magne	8	101	ACGGGTCTTCCTAGCACATCA	CTCGGCGTCGTCGAAGATAAA	ATGGCCAAGGGTGAATTCTAA	TACATGGAGGACGTTACTCAA
PPM1E	protein phosphatase 1E (PP2C	0	141	CCCATTTAGGTCTGTACTAAA	GAGGCGGTTTATAGTCAGAAA	TTGGTTCTATAAACTAGATAA	CCGCCTAATCATGTGTTTATA
PPM1F	protein phosphatase 1F (PP2C	0	142	ATGGTTGGCCACAAACAATGA	CACCTGGTGGTCTGATTCATA	ACCAAGTATTGCTTGGCTTAA	CAGGTGGTGTTAATAAGCCAT
PPM1G	protein phosphatase 1G (forme	8	102	CAGGACCTGAGGACTCAACTA	CCAGAGGATGAAGTAGAACTA	TACTCTGTGAACTTTATTTAA	GAAGTTGTAGATTTCATTCAA
PPM1L	protein phosphatase 1 (formerly	8	103	CAGGACTACGAGAAAGACAAA	CTGGTGGTCTTAGGTCTATAA	AAGCGTGAACCCATATTGATA	CTGTAGAGTCACATATATGAA
PPM2C	protein phosphatase 2C, magn	8	104	ACCGATTAAGGCCACAGGATA	CAAGATAGTAGTATTATTACA	CAGAATATCATATAATGTTTA	ATCGTACTTCTTATTTAGTAA
PPP1CA	protein phosphatase 1, catalytic	17	74	AAGAGACGCTACAACATCAAA	CCGCAATTCCGCCAAAGCCAA	CTGCCTGCTGCTGGCCTATAA	CAGCGAGAAGCTCAACCTGGA
PPP1CB	protein phosphatase 1, catalytic	-17	179	TACGAGGATGTCGTCCAGGAA	TAGGAATATGGTCGGGCTGAA	AAGTATGTTGGTTAATAGGAA	CACTATTGGATGTGATTCTAA
PPP1CC	protein phosphatase 1, catalytic	17	75	AACATCGACAGCATTATCCAA	CTGGTTATAACAGCAAATGAA	CTGCGGTGAAGTTGAGGCTTA	GAGGAGTAAGTGTACAATTGA
PPP1R10	protein phosphatase 1, regulatc	-75	205	CCCAGCCTGCTGAGAAAGATA	CCGAAGGACCGTCACTACATA	CACAGGATCAGCTGCACTTAA	CAGCAACATCTAAGCCCTTGA
PPP1R11	protein phosphatase 1, regulatc	0	143	AACATGAGTAGCGAACACTTA	CGCCCTAACTTTGCTTGCTAA	CAGAGATCAGTCAAATCCATA	TGGCTTGAGATTGGTCACTTA
PPP1R12A	protein phosphatase 1, regulatc	0	144	ATAGTACTCAACCATAATTAA	CAGAATTAACCCGTGAGTTAA	CAGGCAGGCTATGATGTTAAT	AACGAAGAGCTCTAGAAAGAA
PPP1R12B	protein phosphatase 1, regulatc	17	76	CAGGGTGTTGCCTCTAAAGAA	CGGGAGGTAGTAATCCTACAA	CTGGTTGTTGTTATATAGTTT	TAGGAAGATCAGCATATTTAT
PPP1R12C	protein phosphatase 1, regulatc	-8	171	CAGCGGGACCTCAACCCAGAA	CAGGAGGACCTTCGGAACCAA	CAGGCGCTTTGGCCTCCTGAA	TTGGAGGAACTGGCCCGGAAA
PPP1R13B	protein phosphatase 1, regulatc	50	16	CGCGATGATGCCGATGATATT	CGGGCTGAGAGTCCGGTTTAA	CGCCTTAAATAAGTCAGTTAA	ACCAGCGGCGGTGGAGTTAAA
PPP1R14A	protein phosphatase 1, regulatc	-17	180	CCCGATGAGATCAACATTGAT	TTGTATTTAATGGTTCTGTAA	TAATGGTTCTGTAACAATAAA	GCCCAGCTTGCTTGTGTATAA
PPP1R14C	protein phosphatase 1, regulatc	0	145	AAGAGCTGCTTTCTCGGATAA	TAAAGTTGTATGAACCCTTAA	AACCCTTAATTTGAAGAACTA	CCGCAGAAGAAGAGTGTATGA
PPP1R14D	protein phosphatase 1, regulatc	-25	188	CAGGAGCTCTTCCAGGATCAA	CCGCCTGACAGTGAAGTATGA	CAGGCCTGCCCTGAAACTCCA	GAGCCTGAGATTGACCTGGAA
PPP1R15A	protein phosphatase 1, regulatc	0	146	CCAGTTGTTGATCTTATGCAA	TGGGTTTATATAAGGAATAAA	GTGGGTTTATATAAGGAATAA	CAGGATCAGCCGAGGATGAAA
PPP1R15B	protein phosphatase 1, regulatc	-25	189	AAGGTGCTAATTTGGAGCCAA	CAGGGTTACTACCTCAGTTTA	AAGGCTTTGTACAGACAGGTA	CAGGTTTATTGTGTCCTACTA
PPP1R16B	protein phosphatase 1, regulatc	-100	206	ACGGGCGAGAGTAGCAGTGAA	TCGCAGATCTTTGATATCGTA	CAGGCAATTTCGTTCCTGGAA	ATGGAGCTAGTCTCAGTGCAA
PPP1R1A	protein phosphatase 1, regulatc	17	77	AAGGATCACACCCACAATGAA	TTGCCCAGATACATACCTAAA	CAGGGAAGAGTTCTTCCCTTA	GAGGAGGTATCTTGGGATCAA
PPP1R1B	protein phosphatase 1, regulatc	33	35	ATAAATCTTTGTAAATAACAA	CAGCTTGTTTGAAGCCCTTGA	CAGGGATTTGCCCTTCACAAT	CTGAGTCTCACCTGCAGTCTA
PPP1R1C	protein phosphatase 1, regulatc	67	7	CTCGATCTGGAATTACAGCTA	TTGGAACTGGTTAGTACCTAA	TAGGATTTATGTTATAGATAA	AATGAGTTTAATTGACTTCAA
PPP1R2	protein phosphatase 1, regulatc	92	2	CACTACACGTACTGTAATAAA	TACCACTGATTTAGAAACAAA	ATGAGATATATAATCAAAGTA	TTGAATGAGATATATAATCAA
PPP1R2P9	protein phosphatase 1, regulatc	17	78	ACGTACAGAGATTACGATTTA	CTGGAGGGCGGTGGACGGCTA	AACGAAGAATTGAACATCAAA	CAAGATGTGAAGAGAAAGAAA
PPP1R3A	protein phosphatase 1, regulatc	0	147	CACATCAGTATAGGCCATCAA	TCAGGTGGGATTAATTCTGAA	TAGGCCATCAATATCACAATA	CAGAGGAAACTACTTCAAATA
PPP1R3B	protein phosphatase 1, regulatc	17	79	CACCCAAGTTCTTATACGTTA	CCCGCTAGATATGCCATTCAA	CAGACAGTACTTTAAATGTTA	CTAGGATGACATGATGTTATA
PPP1R3C	protein phosphatase 1, regulatc	0	148	TACGATGAATTTCAACGACGA	TCCGGAGAATCAAGATCTTAA	TGGCCTCTTATCGATGAATTA	AGCCTTCAACCGATTACTTAA
PPP1R3D	protein phosphatase 1, regulatc	-50	200	CAGGTACCCACCAACTTTATA	CTGAGTTAGGCAATCACTTAA	AAGGATAGCTTTCTTCGGTAT	TCAGGTGACTAGAGAATTTCA
PPP1R3F	protein phosphatase 1, regulatc	-17	181	CGGGTTGGTACGCGTGCTGAA	AACATGGATGATAACACCTTT	ACCGAAGACCCTGATGATGAA	CACAATAGAGCTCTATGAGAA
PPP1R7	protein phosphatase 1, regulatc	-25	190	CACAAACCCAATGGCAATAAA	TCAGATGCCGTTGCAATTAAA	TTCAGATGCCGTTGCAATTAA	CCAGATCAAGAAGATTGAGAA
PPP1R8	protein phosphatase 1, regulatc	0	149	CAGGCCCAGGAACTGAAGAAA	TACAAATAAAGATGCCCTAAA	CTGCTGAAGTTTCTTATTTAA	AACCCTGAAGCTGTAAATGAA
PPP1R9A	protein phosphatase 1, regulatc	-33	196	CTCCAATGTCAACAGAATTAA	GAGGGTAATATTTATCCTCTA	AAGGATGATTATCTTAAGTTA	CTGCAGTTGGATGGAAATAAA
PPP1R9B	protein phosphatase 1, regulatc	0	150	CAACTCGAAGCTGGTCAGCAA	CCCGGGAGGTGCGCAAGATTA	CACTGAGGAATTCCAATTCTA	CCGGGAGGTGCGCAAGATTAA
PPP2CA	protein phosphatase 2 (formerly	0	151	ATGGAACTTGACGATACTCTA	CAAACAATCATTGGAGCTTAA	ACACCTCGTGAATACAATTTA	CAGATACAAATTACTTGTTTA
PPP2CB	protein phosphatase 2 (formerly	0	152	CCGACAAATTACCCAAGTATA	TGGGATCTGTCTTGGCATTAA	ATGGAATTAGATGACACTTTA	CACCGGATACAAACTACTTAT
PPP2R1A	protein phosphatase 2 (formerly	25	52	ACGGCTGAACATCATCTCTAA	CTGGTGTCCGATGCCAACCAA	CAGAGAAATAAAGGTCTAGAA	TCCCATCTTGGGCAAAGACAA
PPP2R1B	protein phosphatase 2 (formerly	92	3	CAGAAGTTAGGTCAAGATGAA	CAGGAAATAACTACTAAGCAA	CTGACGTTCGTTTGAATATCA	TGGACCAATTCTAGATACCAA
PPP2R2A	protein phosphatase 2 (formerly	-8	172	ATGGAAGGTATAGAGATCCTA	CTGCAGATGATTTGCGGATTA	CTCGCCGTGTCTGGCACTGAA	AAGCGAGACATAACCCTAGAA

PPP2R2B	protein phosphatase 2 (formerly	25	53	CAGGAAATGATTGGAATAGAA	CAGGGACTACTTGACCGTCAA	CCGGAAGATCCAAGCAACAGA	CGGCTACAAATAACCTATATA
PPP2R2C	protein phosphatase 2 (formerly	33	36	ACCGCTCATTCTTCTCGGAAA	CCGGGACTACCTTACAGTCAA	TACTGTCACATCATAGATTTA	GAGGTTATTCTCAGTGGATTA
PPP2R2D	protein phosphatase 2, regulatc	0	153	CAGAGACTACCTGTCGGTGAA	TAGGTGGTTACCACAACAGAA	TTCATCCATATCCGATGTAAA	CCGCTCCATTAAGAACAGTGA
PPP2R3A	protein phosphatase 2 (formerly	8	105	ACCTGTAGTAATCATGAACAA	CAGGAGGATTTCATCCCTCTA	ACCAAGGTAATCAAACTAATA	TAGCATAACATTACCAAGGTA
PPP2R4	protein phosphatase 2A, regula	33	37	CTCCGGGTGGATGACCAAATA	CTGAGGTGGCTGTTTACCTAA	CCGCTCCCTAAGGGTAACCTA	CGGATTCATCCTTACCCTCAA
PPP2R5A	protein phosphatase 2, regulatc	0	154	CAGCGTATTCTGATATAGTAA	CTGTATCATGGCCATAGTATA	CATGGCCATAGTATATTGTAA	CATCAGTATAATATAATTAAA
PPP2R5B	protein phosphatase 2, regulatc	-50	201	CCGCATGATCTCAGTGAATAT	CCGGTTCATCTATGAATTCGA	CCGGGAGCGTGAGTACCTCAA	AAGCCAGGGTGGGAACCCTAA
PPP2R5C	protein phosphatase 2, regulatc	17	80	AACGAGCTGCTTTAAGTGAAA	CCCATTGGAACAAGTAAGAAA	CTGCTACTTCAGTAAGAATAA	CTGGAAATATTGGGAAGTATA
PPP2R5E	protein phosphatase 2, regulatc	-17	182	CACCGGGATTGCAAATCTAAT	CCGGTGATATTGACAATAGGA	CTCGTTCTATATCTCATCACA	AAGGACTTCAATCCAAAGTTT
PPP3CA	protein phosphatase 3 (formerly	-25	191	TAGCGATATAGCATACCCAAA	TCGGCCTGTATGGGACTGTAA	CACGCTTCAGCTACTATCTAA	CTGACATATACTGGAAATGTA
PPP3CB	protein phosphatase 3 (formerly	-17	183	AAGGGTTTGGATAGGATCAAT	TAGGAGATTAGATAGATTCAA	TAGTTTATTGTGAGTACTCAA	CAGCCCGGAAAGAAATCATAA
PPP3CC	protein phosphatase 3 (formerly	25	54	CAGGCTTTCCATCACTTATTA	CCGAGGGTGCTCTTATTTCTA	CTGGACCGAATTAATGAGCGA	CAGGAATAAGATCAGAGCCAT
PPP3R1	protein phosphatase 3 (formerly	-17	184	ATCCTTTAGTACAGCGAGTAA	GCCCATATAATTGGTAATGGA	TCCCTTTATAGTTTCTCTATA	GAGCCTCATGAAGCCAACTAA
PPP4C	protein phosphatase 4 (formerly	-17	185	CGGACAATCGACCGAAAGCAA	TCGCCAGATCACGCAGGTCTA	CTGGACGAGCATCTCCAGAAA	CCAACTGGTGATGGAAGGTTA
PPP4R1	protein phosphatase 4, regulatc	0	155	CAGGCGTTGTTAGATCAGTAT	TGGGAGTGCTGCAGTCTTTAA	AACCTGGTAACTACAAATCTA	CAGCTAGTAATGAGAATGATA
PPP5C	protein phosphatase 5, catalytic	42	24	CCCGTTGGCCCAGTGCATCAA	CTCGTGGAAACCACACTCAAA	CAAGGCCTTCTTGGAAGAGAA	CACGGAGGCCTGTTCAGTGAA
PPP6C	protein phosphatase 6, catalytic	-8	173	CACAAATGAGTTTGTTCATAT	CAGCAGCAAAGTTGTTATTCA	CACCCTGGACTCATTTGAGAA	CTGGTTTGGTCAGATCCTGAA
PR48	protein phosphatase 2A 48 kDa	-50	202	CACGTGTCTCTGTCACGTGAA	CTGGGCCTGAGTGAGCAGTAA	TGCGTTTGTACGGAATGATAA	CACCTTCTTCAACATCGAGAA
PSPH	phosphoserine phosphatase	42	25	CCGGCATAAGGGAGCTGGTAA	TGCCAATAGGCTGAAATTCTA	TAGGCTGAAATTCTACTTTAA	CAGAGACTCATAGCAGAGCAA
PSTPIP1	proline-serine-threonine phosph	-8	174	ACCGGGCGCTCTACGATTATA	CCGGCTGACCATTCTCCGCAA	CAGCATAGACGCCGACATCGA	CAAGAAGGCCATGGAGTCCAA
PSTPIP2	proline-serine-threonine phosph	8	106	CCACGTTATGTCAGCAATGAA	CCGGCTAGTGCTTCTGTGATA	CTCAGTGGTGCAAGATTTAAA	ACGAATAAACTTCTTCCGGAA
PTEN	phosphatase and tensin homolc	-17	186	AAGATTTATGATGCACTTATT	CAATTTGAGATTCTACAGTAA	ACGGGAAGACAAGTTCATGTA	TCGGCTTCTCCTGAAAGGGAA
PTP4A1	protein tyrosine phosphatase ty	8	107	ACGCCTTAACACAGCTCTATA	CCCTTTGATCACGTTAATCTA	CCGACCCGTTGCCATGATTAA	CACGTTAATCTAAATCTAGAT
PTP4A2	protein tyrosine phosphatase ty	8	108	AACAGCATACCTGCTAAGCTA	CAGAGAATGCTGGTAGCTTAA	ATGCAACAATAGATTCCATTA	AGGGACTGTGTTGCTTGTGAA
PTP4A3	protein tyrosine phosphatase ty	0	156	CACCCAAGTATTTGCACAATA	CCGCGGAGCCATCAACAGCAA	CACCTTCATTGAGGACCTGAA	CCGGTGGAGGTGAGCTACAAA
PTPDC1	protein tyrosine phosphatase d	17	81	CGGAATGTTGAGTGCCTTCAA	TACGTAGATACCAGAGGCCAA	AGGCTATACATAAGTATTGTA	AACAGAGGGTTTCAAAGCATA
PTPLA	protein tyrosine phosphatase-lik	17	82	ACCACTTGCCATACTTCATTA	CACTGTTTAATTGGAATTGTA	CTGGTGAACTTCTTACAATAT	AAGTGAGTTCAAGAATCTTTA
PTPLB	protein tyrosine phosphatase-lik	8	109	CACGGCGTACCTGGTCATCTA	CAGCCAAGAAATAGTTTGGTA	TACGCTTAACTTTCTATGCAT	TCCTATGTTAATTTCCACCAA
PTPN1	protein tyrosine phosphatase, n	25	55	CACGTGGGTATTTAATAAGAA	CAGGCATGCCGCGGTAGGTAA	CAGGAATAGGCATTTGCCTAA	ACGGACGTTGGTTCTGCACTA
PTPN11	protein tyrosine phosphatase, n	75	5	CAGAAGCACAGTACCGATTTA	CCGCTCATGACTATACGCTAA	GCGGTCCAGCATTATATTGAA	GCCGCTCATGACTATACGCTA
PTPN12	protein tyrosine phosphatase, n	50	17	AAGCTTAATGAGGAAATATCA	TTGCAGGTTATCAGAGATCAA	CTGCTTGTAGACATGTTAATA	GTGGATCATGATAACACTTCA
PTPN13	protein tyrosine phosphatase, n	83	4	CGGTCTATTCTTACTAAGAAA	TCCAGGTACATTAAAGATGAA	TCGATGGATAAGTATCATATA	AACCTTTGGATCAGTGTCTAA
PTPN14	protein tyrosine phosphatase, n	58	11	AAGGGCGATTACGATGTACAT	CGGTGTGGCATTTACAATATA	CTGGCCCAAACTAGGTTCAAA	TCGGTGGAAAGCACAGGGCAA
PTPN18	protein tyrosine phosphatase, n	69	6	CAGGCAGACATCAGTCCACAT	CCCAATGACTGTAGCATTCAA	GTGGGCCTGGATCAAAGTTAA	CCGGGTGTAAGTCTAACGCCA
PTPN2	protein tyrosine phosphatase, n	0	157	AACTGTATTCATACATGTCAA	CCGCTGTACTTGGAAATTCGA	TCGATTGAATTGTACTGGATA	CACAAAGGAGTTACATCTTAA
PTPN21	protein tyrosine phosphatase, n	8	110	GAGGAGACCATTCAATTTCAA	GTGCATAGATTTCTATCTTAA	AAGCACCTCCTTACCGGGCAA	CCCACCGCAGTTGCACTATAA
PTPN22	protein tyrosine phosphatase, n	8	111	CCGGGTAGAACTATCCCTGAT	TGGGATGTACGTTGTTACCAA	CCCAGGGTCCTTTATCTACAA	TACGTAATGCCTCTAATGTAA
PTPN23	protein tyrosine phosphatase, n	-25	192	AACCTTGTACAGTCCATGCAA	CCGCCAGATCCTTACGCTCAA	CTGCGTGAGCTTATCCAGAAA	CCGGCCCGACACTGTCAGGAA
PTPN3	protein tyrosine phosphatase, n	8	112	CAGGTTATTCAGCGATAGTTA	CCGGGTATTATTGCAGGGAAA	CCGAGAAATGCTGGTCACAAA	CCGCTCATTTGCTGACTTCAA
PTPN4	protein tyrosine phosphatase, n	67	8	CTCCGAACAAATAGTAAATAA	TCCGTCATCAACACAAGCTAA	CTCCGTCATCAACACAAGCTA	AGCACGTACCTTAGAACTCTA
PTPN5	protein tyrosine phosphatase, n	0	158	ATCGAGGAGATGAACGAGAAA	CACCAACATCGAGGAGATGAA	CAGCTGAGGGAGAGTTCTCTA	CCCTCTGAGTTCCTACATCAA
PTPN6	protein tyrosine phosphatase, n	25	56	CCGGAACAAATGCGTCCCATA	TAGGCCCTGATGAGAACGCTA	CCGCACCTCGTCCAAACACAA	CCAGTTCATTGAAACCACTAA
PTPN7	protein tyrosine phosphatase, n	-50	203	CAGGTCTACCTCAGGACTGAA	CTGGCATTTATGACAGACAAA	AAGCTCCAGAACAGTAACCAA	CACCCATGTGTCATAAGAGTA
PTPN9	protein tyrosine phosphatase, n	0	159	ACCAAACTAGAGTGAAGCTAA	AGGAACGGAGCGAATAATATA	CCAGTAGCAATGTGTTCTTAA	CAAGTGGACAGTTCAGTACAA
PTPNS1	protein tyrosine phosphatase, n	0	160	CGCCTGTAAATTACTGAGAAA	CTCGCTGTGGACGCCTGTAAA	ACGCCTGTAAATTACTGAGAA	CCCGAGAAGAATGCCAGAGAA

PTPNS1L2	protein tyrosine phosphatase, n	0	161	CAGGGCCAAACCGGAAATTAA	CCGGAAATTAATCTACAATTT	AAGGTAACTTTCCCAGAGTAA	AAGCTCCAGGTTTCACCACAA
PTPRA	protein tyrosine phosphatase, r	42	26	CAGAGTGATCATTCCAGTTAA	CCGGAGAATGGCAGACGACAA	CAGGTGTAGGGCGTACAGGTA	AGGCATTACAATTTCACCAAA
PTPRB	protein tyrosine phosphatase, r	8	113	CCCGGAGATGTGGATAACTAT	CCGGTCGACTTTATCAAGTTA	TCGGGTGTATCAGACTAATTA	CCAGTATTAGTGGAGACTTAA
PTPRC	protein tyrosine phosphatase, r	8	114	AACCGTTATGTTGACATTCTT	AAGAATTGCGATTTCCGTGTA	TCGATTATTCCCTGTACAATA	CAACTTCTTTGTAATCGTTAT
PTPRD	protein tyrosine phosphatase, r	-17	187	ACGGCCAGTCCCGAACAGTAA	CTGGGTGTCATTGAAGCAATA	CGCCTTGTTAATATTATGCCA	ATGGCATTATCACCAAGTATA
PTPRE	protein tyrosine phosphatase, r	25	57	ACCACGGGCAATTAAACTTTA	CCGAGTGATCCTTTCCATGAA	CAGTGAATTCACAACCCTGAA	GACCATCGTCATGTTAACAAA
PTPRF	protein tyrosine phosphatase, r	0	162	CAGCGCTATCTAGATAGGTAA	CATCGTGTTTGCAAAGGTTAA	CCGAGGACTATGAAACCACTA	CAGGAGCGGATCATCATGTAT
PTPRG	protein tyrosine phosphatase, r	25	58	AGGGTGAAGTTAAGACCTTTA	TCGGTGAGCTCTATTCTAATA	TAGGCACTGTTCAATACTGTA	CAGACTCTAGGTTATACAATA
PTPRH	protein tyrosine phosphatase, r	0	163	CCGGGACGTTGTACAATTTCA	CCGGGTCATTGTATACGTGTT	CAGGTACTGACATCACCCTAA	TCGAAGCACAGCACACACTAA
PTPRJ	protein tyrosine phosphatase, r	33	38	TCCGAGTATGTCTACCATTTA	TCGGGTAGAAATAACCACCAA	ACGAGTCGTCATCTAACTATA	ACCCGTATCTTCTACAATCAA
PTPRK	protein tyrosine phosphatase, r	25	59	CCGGGTTAAATGCTATAAATA	CTGGAGATTAGTGTATGATTA	CCGGCGAGTCAAGTTATCAAA	CAGGATTTGTATCGCTGTGTA
PTPRM	protein tyrosine phosphatase, r	8	115	AAGGGTCAAATGCTGCAAATA	CACATCCGTAGTTATGCTAAA	CAGGATATTCCGCATTTACAA	CACCTTTGAATCAAACTGACA
PTPRN	protein tyrosine phosphatase, r	8	116	CACCCTTCACTGAGTTACGAA	CAGGTCTGGCTTGGCACCCAA	CAGGAAGGTGAACAAGTGCTA	CTGGTGAAGTCTGAACTGGAA
PTPRN2	protein tyrosine phosphatase, r	25	60	AAGGTGCTAAAGAGATTGATA	CAGCGCAGTTTAGCAGTTAAA	AGCGGACAGAATGATGCCAAA	ACGGATGTTGTCAGGAATCAT
PTPRR	protein tyrosine phosphatase, r	17	83	CGCCACCAGATTGTCAATTCA	TCGCCTCATTGGAAAGAAGAA	TAGGTTTATCACACAGCCTAA	AACCCTTTGTGTCTATACCAA
PTPRS	protein tyrosine phosphatase, r	100	1	CACGGCATCAGGCGTGCACAA	CGCGTCTACTACACCATGGAA	CAGGACATTCTCTCTGCACAA	AAGAACAAACCCGACAGTAAA
PTPRV	protein tyrosine phosphatase, r	50	19	AACGCTGAAGCAGTATATCTA	AAGGTGGGCAGTCATGTCCAA	ATCCCTTTCCATGGGCATAAA	ATGCCACAGAGTGGACCTATA
PTPRZ1	protein tyrosine phosphatase, r	42	27	ACGCTGGAATTTGGTAGTGAA	TAGCCATATACCAATACCTAA	CCGCCAAATTTATATCATTAA	CAGACTAATTACACTGAGATA
RNGTT	RNA guanylyltransferase and 5'	33	39	CAGGGTTGTTAAGTTGTACTA	CGGGATTTCTATATGGACATA	TACCATCTGCAGTATTATAAA	ATGGATTTAAAGGGCGGCTAA
SBF1	SET binding factor 1	0	164	CAGCGCCGAGCTCTTCCGTAA	CCGCGTGGTGTGGCCCTGTTA	TCCGGTCGTTACCGACCACTA	GACGCCTGTGTTCCACAATTA
SGPP1	sphingosine-1-phosphate phosp	0	165	AGAGATTAACTTTCCATATAA	ATCGGTATATTACCTATGGAA	CTGCCATTACCTTTCATGTTA	TGCGTAATTACTAGACCAGAA
SKIP	skeletal muscle and kidney enri	-33	197	CAGCCAAGTGTCGTCCACATA	CTGGAATTAGCCGCTTAAATA	CACGTTCGACTTGGAGCTGAA	ACGGTCGGAGTCCGGAAGAAA
SNAP23	synaptosomal-associated prote	0	166	CTGGCAAGGCTTATAAGACAA	CAGGCCTATTAACATCATACA	TACCACATGAATTCAGATTTA	AAGAGGTTGTTACCTCAGTAA
SPAP1	SH2 domain containing phosph	42	28	TCAGAAGATGGCTTACCATAA	TTCAAATATAGTAAAGATAAA	CAGGACCTGATGGCTATAGAA	ATGCCGGCAAATATTACTGTA
TA-PP2C	T-cell activation protein phosph	17	84	AAAGGGATGGTACAAGTCTAA	CACAAATTGTACGTAATGATA	CCCTCAAAGCCTAGAAATTTA	CTCAATTCTCAGGGACTTTAA
TENC1	tensin like C1 domain containin	-8	175	ACAGCACGTGGTCGTACTATA	CAAGGTGGCGACGCACAGAAA	ACGGCCATCCTAGATGACGAA	CTCGGTCTCTGTCGACTACAA
TPTE	transmembrane phosphatase w	25	61	CAGATTGGCAACCAAGACTAA	CTGAAATATGTTCAACTGCAA	TCGGTACTTGATAACATTACA	CAGACTTGTGTTATTCTAGCA
TPTE2	transmembrane phosphoinositi	25	62	ACCTGGAGAACTGATAATAAA	CTGATAATAAATTGTGGTTTA	ACAGGCAAATTTCAGAAACAA	AATGATTGAAATAGAGCTATA

Table S1. siRNA-mediated knockdown of human phosphatase genes alters cellular PI(3)P. U2OS-EGFP-2xFYVE cells were transfected with siRNAs targeting human phosphatase genes for 48 h (4 siRNA sequences per gene per well; all four sequences displayed). Following knockdown, EGFP-2xFYVE signal and distribution was visualized by confocal microscopy and scored from -100 (decreased punctae from control cells) to +100 (increased punctae) and means determined. Select genes were validated using multiple unique siRNA sequences and their efficacy was incorporated into their scores (see *Methods*). Genes were ranked based on their scores from 1 (most increased EGFP-2xFYVE) to 206 (most decreased).